

This is an updated version of our response to Referee 1. Our response and changes to the manuscript are indicated separately, and Referee 2's comments have also been considered in the responses below. Referee comments are in black, author responses are in green, and manuscript changes are in blue.

General changes:

We made some manuscript changes that are not based on the referee's comments. These are:

- RHic (which was meant to stand for RHi climatology) has been changed to RHib (background RHi) for consistency with the terminology used in the discussion.
- In the submitted manuscript, we have used data within 1 Nov 2006 to 30 April 2014. We think that this causes an uneven sampling in season, which could affect the results of Figure 5. For this reason, in the revised version we plan to remake Figure 3-7 and Figure 9 using data within 1 Jan 2007 to 31 Dec 2013, so that the number of sampled months in each season is the same. After making this change, the largest change in percentage is 3% in Figure 3 and 1% in Figure 4.

Specific Comments (by Line Number):

45: Your narrative suggests P18 agreed with K16 in placing the highest cloud frequencies in phase 1 of the gravity wave perturbation cycle. But in P18's figure 3, large ice crystals can also be found in phase 3 (where they are sublimating). Putting aside the effect of background relative humidity, P18's abstract says "The precise location where the confinement (i.e., wave-driven localization of ice crystals) occurs ... is always characterized by... a positive vertical wind anomaly." So while P18 agrees that ice is suspended in phase 1, I would mention their finding that upward vertical motions permitted the presence of TTL ice clouds within phase 3 as well.

Author Response: Based on Referee 2's response to this point, we have decided to leave the sentence as-is.

Manuscript changes: At line 190 we mention that in Phase 3 the upward vertical wind anomaly may play a role in it having more clouds than Phase 4.

76: Why is the effective vertical resolution of RO profiles ~200m when temperature estimates are given at 30m spacing? Are the temperature data too noisy, and require vertical averaging? Are you using a version of the RO temperature retrievals that removes fine scale artifacts?

Author Response: It is probably more appropriate to say that the vertical 'weighting' is ~200m. At each height, the vertical weighting is more or less centered on the reported height in atmPrf, so each height has a slightly different vertical weighting even though they are only ~30m apart. In other words, the RO temperature can be interpreted as a temperature profile with a

smoothing window applied, with the width of the window as the vertical weighting.

Manuscript Changes: No changes.

90: Explain what a “retrieval to flight ratio” means. Is that the ratio of the satellite-retrieved r_e to that determined from aircraft measurements? How does the +/- 20% uncertainty of retrieved r_e values compare with those derived from in-situ flight measurements?

Author Response: Yes, the ratio is the satellite-retrieved r_e divided by the r_e derived from in-situ 2D stereo probe measurements. The 1.05 is the mean ratio and we have revised the paper to indicate ‘mean retrieval-to-flight ratio’. It is hard to know how our choice of +/- 20% uncertainty compare with in-situ measurements. At line 280 we have noted that retrieval of r_e has large uncertainties especially with respect to thin cirrus., so that the reader is aware of the associated uncertainties in our results pertaining to r_e .

Manuscript Changes: No changes.

140: How large is the sample of CALIPSO cloud profiles corresponding to each RO profile? In terms of the spatial collocation criteria I’d like to see the results of a sensitivity analysis, where you try both a smaller- and larger-sized diameter range with respect to the RO perigee point. Depending on sample size, I might try 50 km and 200 km and see if your results are affected in any significant way. A larger diameter incorporates more data, which is statistically preferable. But as wave phase surfaces slope with increasing distance from the RO perigee point, a smaller diameter mitigates the possibility of associating the presence of clouds with the incorrect phase. Bound by these constraints, what spatial collocation criteria is optimal?

Author Response:

Figure 2 below shows the distribution for how many CALIPSO profiles tend to be collocated to be each RO profile. There is a sharp cutoff at around 40 profiles. Since each CALIPSO profile has 5-km horizontal resolution, $40 \times 5\text{km}$ is 200 km which is consistent with the 100-km radius collocation criterion.

As you say, a smaller diameter is probably more preferable since it is less likely to be influenced by sloping wave phases. We have done some testing using 50 km and 200 km as a collocation radius. As a reminder, the radius used in the manuscript is 100 km. Please see below for the cloud population in phases obtained using these collocation radii.

For altitudes below 17.5 km, the results from using 50 km vs 100 km (Figure 3 in this document vs Figure 1), the difference is at most 1%. Above 17.5 km, there are larger differences, but the number of samples is quite small at this altitude. Overall, there is good agreement between using 100 km and 50 km, which is reassuring. Results from using 200 km (Figure 4) remains qualitatively similar, but we see 2% differences (53% vs 55% in Phase 1 in panel (a)).

It is hard to objectively assess what collocation criterion is optimal. However, here we show that the results are not particularly sensitive to the collocation diameter. The qualitative features remain largely the same. Since 100 km provides more samples than 50 km, we prefer to maintain the use of 100 km. We will mention that we tested these collocation radiuses and the results had small variations in the text.

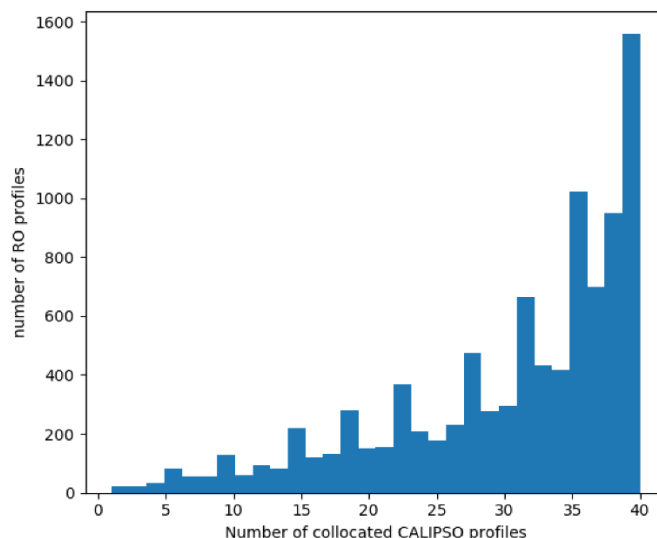


Figure 2. Distribution of the number of CALIPSO profiles collocated to RO profiles. The collocation criteria are 100-km radius and +/-2 hours.

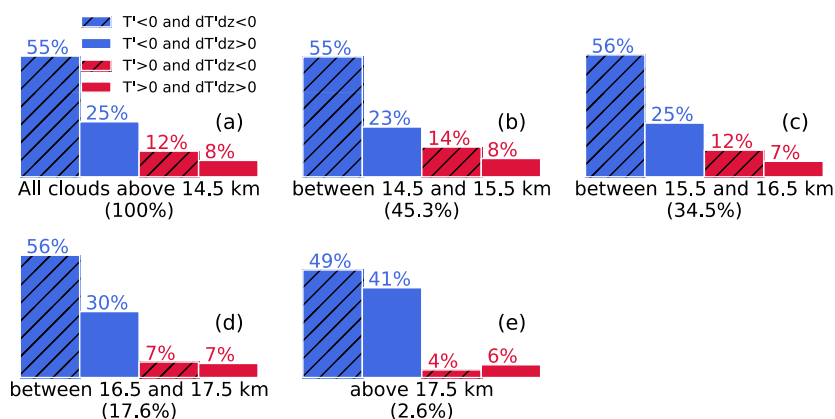


Figure 3. Same as Figure 1 except made with collocation radius of 50 km.

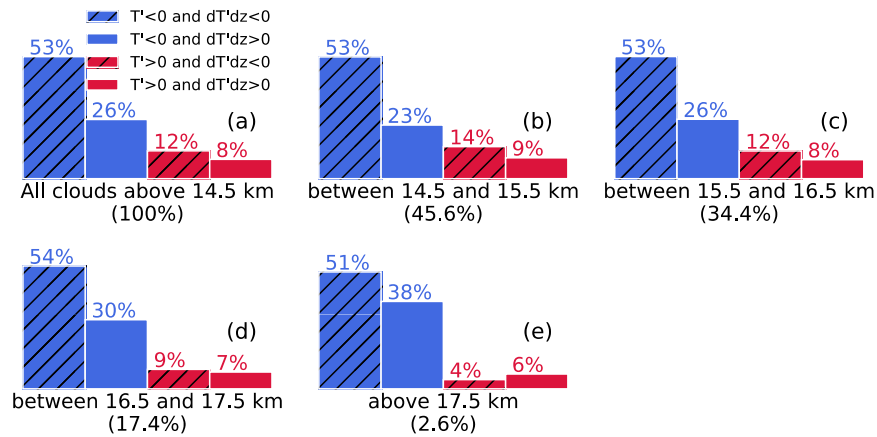


Figure 4. Same as Figure 1 except made with collocation radius of 200 km.

Manuscript Changes: No changes.

145: What is the mean (and standard deviation) of tropopause altitude in your RO dataset? It would follow that convective detrainment would only occur below this level; is this consistent with your finding that warm phase clouds decrease markedly above 16.5km? Or above an even lower altitude? Does this impact your comparison with K16's cloud fraction results? How so?

Author Response:

The mean and standard deviation of the tropopause within 20N/S of the equator is 17.14 and 0.72 km. For a detailed discussion on the differences of clouds above or below the tropopause, please see our response to the next comment. In summary, below the tropopause we find more clouds in the warm phase, consistent with the expectation that convective detrainment occurs below the tropopause level.

In K16's Figure 5, they showed that the T' of low clouds (below 16 km) associated with convection were distributed evenly across the four phases, while clouds non associated with convection were more common in Phase 1 and 2. Although we are not able to separate convective and non-convective clouds, our results here are consistent with their findings.

Manuscript Changes: No changes

155: I think it would be worth re-running this analysis, having deleted altitudes that are below the mean tropopause for each geographical region and season. Does this reduce the influence of deep convection that is likely impacting your results for the western Pacific winter, or the Asian monsoon region during summer? Then either update figure 4 with new "filtered" results or else explain the difference (or lack thereof).

Author Response:

We have updated Figure 5 to include the cloud population above the tropopause. The

mean tropopause for each longitude band and season was calculated using RO. There are generally less clouds in the warm phases and more in the cold phases when looking only above the tropopause. In the western Pacific winter region, there is a significant reduction of clouds in the warm phase. The reduction is less apparent in the summer Asian monsoon. One possibility is that the tropopause is elevated by the upper tropospheric anticyclone (associated with the monsoon), causing outflow clouds to be present at higher altitudes. In Section 4.1 we will add discussion regarding the exclusion of clouds below the tropopause. Manuscript Changes: Changed Figure 4, and also changed the discussion in Section 4.1 regarding this figure.

165: In regards to your comparison with K16's ATTREX results, I recommend re-computing your RO-derived T' values using a 30-day rather than a 7-day mean temperature. Does making this change result in a significant difference? Please see Figure 6 below for the cloud population derived using 31-day mean temperature. Compared to the population derived from 7-day means, there tends to be slightly more clouds in the Phase 1 and less clouds in the warm phases. Unlike what K16 found, we do not see that Phase 2 having more clouds than Phase 1 in the 180W-120W band. In paragraph 4 of Section 4.1 we will add a note that we tried using the 31-day mean and explain what we found.

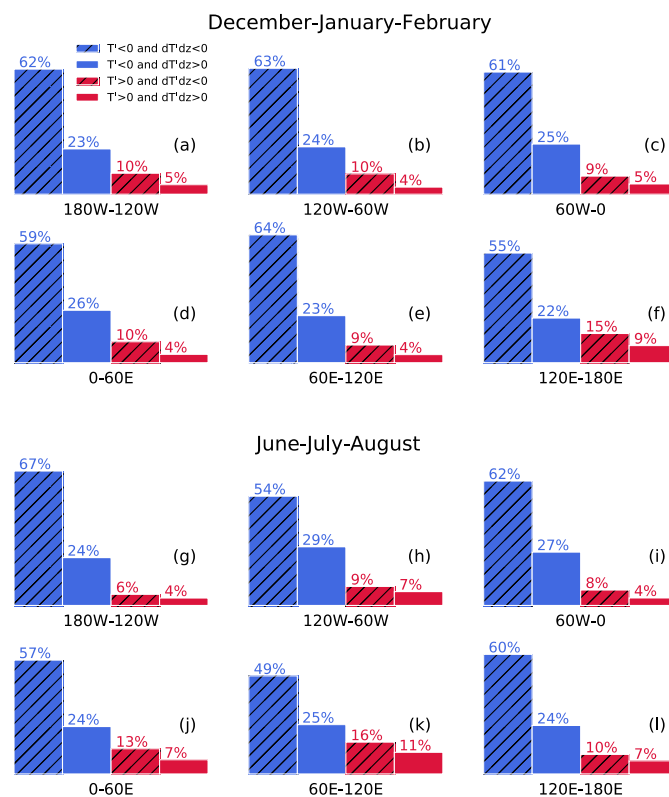


Figure 6: Same as Figure 4 in the manuscript, except derived using 31-day mean temperature as background state.

Manuscript Changes: Added discussion regarding the use of 7-day mean vs 31-day mean at the end of the 4th paragraph in Section 4.1 (around line 175)

168: Re-word “line segments in Figure 1 according to each phase.” Do you mean “...defined as the amount of vertical overlap between individual cloud boundaries and wave phases?” For example, what if a profile’s Phase 1 region extends from 14.8 – 15.2 km, but the cloud layer product indicates a cloud only from 14.9 – 15.1 km. In that layer, is $CF = 0.2\text{km}/0.4\text{km} = 0.5$?

Author Response: Yes, we mean that it is the amount of overlap between individual cloud boundaries and wave phases, as you stated. We have edited the sentence to state this. Your example is correct, in that case the CF is 0.5.

Manuscript Changes: Added an example like the one here at line 179 of the revised manuscript.

Table 1: I wonder if this is necessary or can you just incorporate this information into the text? If you keep the table, I would (at least) eliminate the CF=0 column, and explain why the number of cases where CF=1 far exceeds the number of cases for which $0 < CF < 1$ (shown in figure 5).

Author Response:

For Table 1, we have decided to put the total count of $0 < CF < 1$ in place of the C=0 column, and in the CF=1 column we have added a percentage showing the fraction of instances with CF=1.

As for why CF=1 tends to outnumber cases with $0 < CF < 1$, see Figure 7. We find that the vertical thicknesses of the Phase 1 (distribution in blue) tend to be smaller than the typical cloud thickness (black). Since clouds are thicker, it is likely that the entire Phase 1 is embedded in clouds, hence the higher frequency.

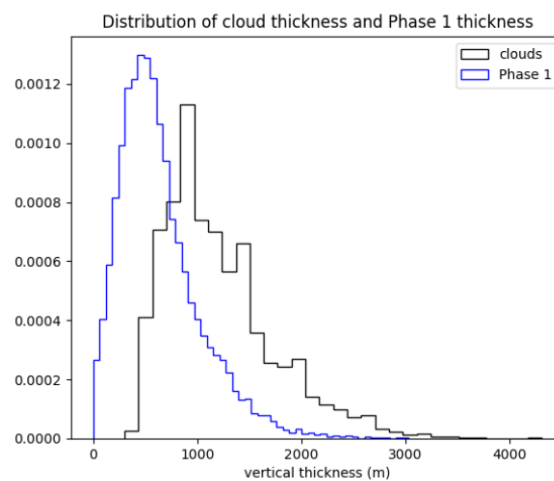


Figure 7: Distribution of Phase 1 vertical thickness (of those used to derive Figure 5 of the manuscript), and the thicknesses of clouds that overlap with Phase 1 (black)

Manuscript Changes: Modified Table 1 and discussion regarding this table.

207: Are the weak anomalies of figure 7 simply the result of variability in sampled cloud top heights diluting the overall result? Explain.

Author Response: Yes, the weak anomalies are a result of cloud top height variability. Since it is common that TTL clouds are embedded in Phase 1, their cloud tops tend to be close to the T' minimum (this is depicted in Figure 6). Since we don't composite with respect to the cloud top height in Figure 7, the result is a pattern of weak anomalies.

Manuscript Changes: No changes.

221: How can you compute cloud fractions with 50m vertical spacing when the CALIOP 5 km cloud profile product only reports the presence of cloud every 60m?

Author Response: When the CALIPSO product reports the presence of a cloud in a bin, we are assuming that the cloud occupies the entirety of the bin. Say that the CALIPSO product reports that a bin at height z has a cloud. Then we assume that the region between $z_0 = z + 30\text{m}$ and $z_1 = z - 30\text{m}$ is occupied by a cloud. Then, in the grid on which we calculate the cloud fraction (the grid has 50-m spacing), we check the overlap of the cloud boundary $[z_0, z_1]$ with each bin on the grid. In this approach, the two spacings do not need to match. Because the reported CALIPSO heights are not on a regular height grid, there isn't much advantage in using a 60-m grid since the same method would have to be used.

Manuscript Changes: No changes.

238-250: This explanation seems overly detailed and tedious. I would shorten this narrative, focusing on your statistical goals, and eliminate Figure 9(g)-(i), since these panels just look like averaged cloud fractions within the column, and show very minor differences between them. I would attempt to make the remaining 12 panels of figure 9 each a little bigger for visibility.

Manuscript Changes: We have moved the explanation (most of lines 238-250 of the submitted manuscript) to the appendix, and in the main text we briefly summarize that we extract the anomalies by building a background cloud fraction. Figure 9(g)-(i) has been eliminated from Figure 9.

272-281: I'm surprised that distributions of re from 2C-ICE data are so uniform. I doubt that the difference between altitude bins is significant. I'd prefer that in figure 10, you keep the results for all TTL altitudes (panel (a)), but delete the vertical stratification presented in panels (b)-(d). Instead, I'd like to see three panels of re distributions from a more limited temporal and spatial domain (but for all altitudes combined), namely: (a) the region from 180W-120W during DJF; (b) from 120E-180E during DJF; and (c) from 60E-120E during JJA. Then as per figure 4, discuss whether convective influence might have an impact on observed

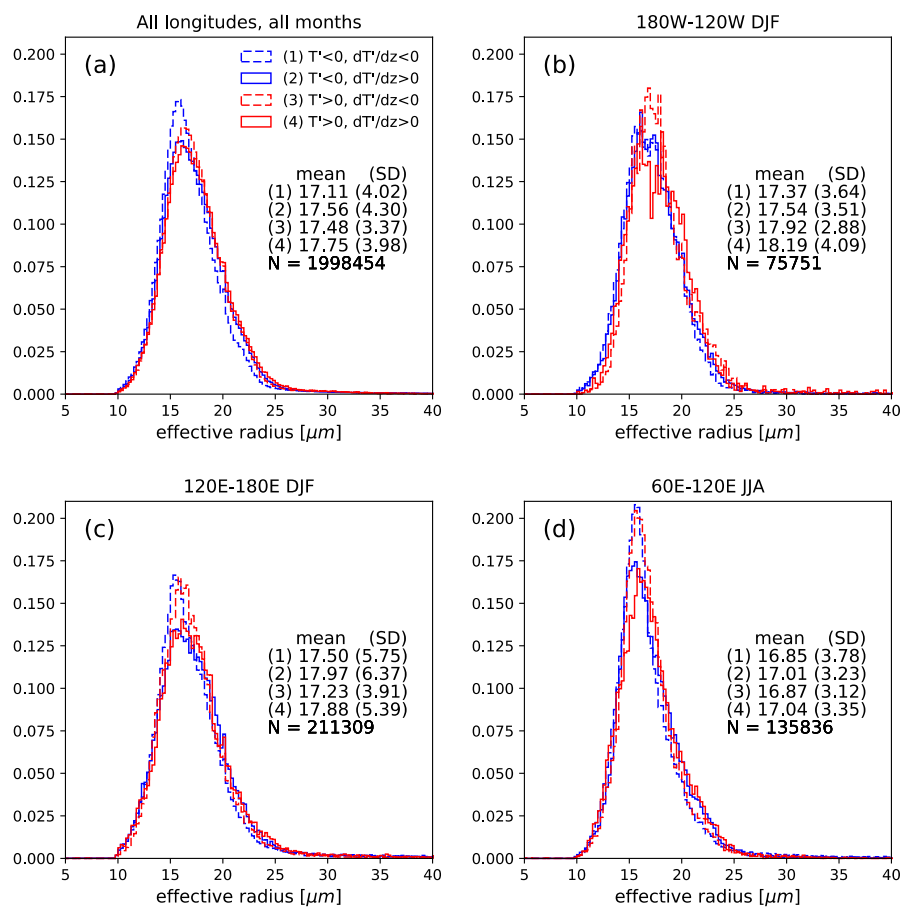
ice crystal sizes.

Author Response:

We have reproduced the r_e distribution as you specified (shown below) The regions associated with frequent convection (120E-180E DJF and 60E-120E JJA) exhibit a lower mean r_e in Phase 1 and 3. The r_e distribution of these phases also tend have a higher peak compared to Phase 2 or 4. However, it is not clear whether this is a result of convection or not. One might have expected to see larger r_e in these regions due to detrainment, yet this is not observed. An interesting feature is that the distributions over 60E-120E JJA are notably narrower than those of 120E-180E DJF, but this feature seems independent of the wave phase.

In the previous response to Referee 1, we wrote that we will use this new figure in the paper. However, the new figure does not suggest any significant influence from convection, so the results are inconclusive. Considering this, we decided to keep the original Figure and discussion.

Manuscript Changes: Added number of r_e samples to Figure 10, and updated the bin widths (all distributions now have the same bin widths).



329: I would interpret this a bit differently. I think there is a clear trend in partitioning between phases 1 and 2 from low RH_{ic} values, up to 100%. Thereafter it makes little difference, except for the highest supersaturation values.

Author Response This is an interesting point. Figure 11 has been remade into a line plot to better show the cloud population as a function of RH_{ib}. RH_{ib} is now binned in 0%, 50%, 60%, 70%, ..., 180%. The 0% to 50% is grouped together because of the low number of samples. As shown below (Figure 9), there is a rather apparent trend in Phase 1 from 50% to 100% as you noted. On the other hand, Phase 3 and 4 don't seem sensitive to RH_{ib}. Phase 2 also exhibits a decreasing trend as RH_{ib} increases up to 100%. In the text, the discussion has been edited for this new figure.

Manuscript Changes: Updated Figure 11 and subsequent discussion.

Technical Corrections:

Title: Suggest "Influence of a gravity wave temperature anomaly..."

Manuscript Changes: Title was changed to "Influence of gravity wave anomalies and their vertical gradients on cirrus clouds in the tropical tropopause layer -- a satellite-based view"

183: Try "-35, -33, ... , -1, 1, ... 33, 35"

Manuscript Changes: Changed as suggested.

Figure 4: Can you include the number of profiles that contain clouds for each latitude bin?

Manuscript Changes: We have added the number of CALIPSO Cloud Profile bins included in each plot. The number is shown under the longitude label. Note that this isn't the same as the number of profiles since one profile may have multiple bins with clouds.

298-300: Try something like, "We conclude that our analyses of re and RH_{ic} data is qualitatively consistent with P18's results."

Manuscript Changes: Changed as suggested.

345-348: Suggest, "...as well as upward vertical motion all impact wave anomalies (...), it remains to be determined whether one has a stronger role in favoring cloud formation."

Manuscript Changes: Changed as suggested.

Figure 11: Add percentage symbols (%) to each of the RH_{ic} labels and add the number of cloud encounters each panel represents.

Manuscript Changes: This figure has been changed from bar plots to line plots showing cloud population as a function of RH_{ib} (see Figure 9 above). The number of cloud bins in each RH_{ib} category is also shown in the bottom plot.

Response to Referee 2's comments

Thank you for the feedback on the submitted manuscript and Referee 1's comments. We have adopted most of your suggestions, as detailed below. Referee comments are in black, author responses are in green, and manuscript changes are in blue.

Minor comment:

Contrary to Kim et al (2016), the authors show the distribution of clouds between the different wave phases instead of the mean cloud fraction in each phase. The former can be deduced from the latter (which the authors do on page 6 line 148), while the reverse is not true. I am a bit puzzled by this choice which appears to result in a reduction of the information conveyed by the figures.

Is it motivated by the sensitivity of the mean cloud fraction to the CAD threshold used to distinguish clouds from aerosols? By the fact that the cloud fraction depends on CALIOP optical depth detection threshold? Or is it just meant to facilitate the visual and quantitative comparison between regions/altitudes with different cloud fractions? Some explanation would be welcome.

Author Response: With aircraft observations as in Kim et al. (2016), they can obtain the cloud fraction in each phase, presumably by dividing the number of observations with clouds by the total number of obs. With CALIPSO observations, the 'total' number of observations is somewhat arbitrary. For example, if we define the total number of obs to be all CALIPSO bins within 14.5 to 20 km, then the cloud fraction in all phases will be quite low, since above ~17 km most CALIPSO bins will have no clouds. As you can see the 'cloud fraction' derived this way can vary a lot depending on the TTL height bounds, so we decided to look at the partitioning among phases, which is straightforward to interpret.

Manuscript Changes: No changes made for this comment.

Specific comments

Page 2, line 44-46: A clarification here related to Referee 1's comment: "while P18 agrees that ice is suspended in phase 1, I would mention their finding that upward vertical motions permitted the presence of TTL ice clouds within phase 3 as well" and the authors reply. Actually, the interpretation in the submitted manuscript was correct: P18 indeed claim that phase 1 is more favorable for cirrus than phase 3. Referee 1's confusion lies in the choice of words in the quoted sentence. The exact P18 sentence reads: "The precise location where the confinement occurs ... is always characterized by a relative humidity near saturation and a positive vertical wind anomaly". The effect of relative humidity cannot be put aside to correctly interpret that sentence. Indeed, relative humidity near or above saturation is mostly found in negative temperature anomalies (Phase 1 or 2) while the vertical wind is positive in phases 1 and 3. Taken together, the two conditions mean that clouds are found in phase 1. This is illustrated by figure 2 of P18. Note that the sketch in their figure 3 was meant for purely pedagogic purposes, showing possible cases.

Author Response: We will leave this sentence as-is, since the interpretation is consistent with P18

Manuscript Changes: No changes made for this comment.

P3 line 83-85 : Are the results affected by the choice of the CAD threshold ? By how much does the average TTL cloud fraction estimate vary depending on this threshold?

Author Response: The choice of CAD fraction doesn't affect the cloud fraction much. In terms of the percentage of all TTL clouds in each phase, a threshold of CAD ≥ 80 results in 53.4%, 25.9, 12.2, and 8.5 for Phases 1,4, while CAD ≥ 90 yields 53.4%, 26.1%, 12.1%, and 8.5.

Manuscript Changes: No changes made for this comment.

P3 lines 88-92 and fig. 10 : I believe that in most thin TTL cirrus there are only Lidar measurements available (their reflectivity is below the radar detection threshold), so that re cannot be unequivocally determined. This might explain why the 2D ice data are so uniform

Author Response: Yes, it is true that radars miss most of the thin TTL cirrus. Aside from this, their being very optically thin also poses challenges in constraining the retrieval.

Manuscript Changes: No changes made for this comment.

P5 line 128-130: This is more of a sanity check, but are all 4 phases equiprobable?

Author Response: Yes, we've done some checks and found that the number of samples across the four phases are more or less evenly distributed.

Manuscript Changes: No changes made for this comment.

P6 line 147: you should specify that K16 measurements were made in the Western Pacific

Manuscript Changes: Added the clarification starting at line 152 of the revised manuscript.

P7 lines 160: The contrast remains, but I would say that K16 found "slightly" more clouds in phase 2 (6 % vs 5 % in phase 1).

Manuscript Changes: Added "slightly" in the at line 170 of the revised manuscript.

P7 line 172 and Figure 5: Instead of the count (number of layers?), would it be clearer to show some "phase fraction" (i.e. normalized by cumulated altitude)? I am unsure myself.

Author Response: You are correct that the count is the number of layers. We added an example of how the cloud fraction is calculated, in hopes of making this part clearer. We don't quite understand what is meant by showing phase fraction normalized by cumulated altitude, and decided to leave the figure as-is.

Manuscript Changes: Added an example of the cloud fraction calculation at line 180 of the revised manuscript.

P8 line 177-182: I like the composite approach, but it might be worth mentioning that, by essence, it is stationary in space, so that neither the cloud (moved by the wind) nor the wave anomaly

(moving at the wave phase speed) are followed. For instance, if the structure moves at 10 m/s, 30 hours corresponds to a displacement more than 1,000 km (10 times the collocation radius) away from the location where the composite is made

Manuscript Changes: We added a sentence in the conclusion (line 351) to note the stationary nature of this technique.

P10 lines 202-203: I don't think the roles of the wave through its impact on stability and on vertical motion can be easily disentangled. They necessarily hold at the same time, as a consequence of the polarization relations.

Manuscript Changes: We modified this sentence here to be : "Since negative dT'/dz also corresponds to upward vertical motion anomalies (assuming that these anomalies are from gravity waves), it is difficult to separate the effects of each on cloud formation."

P10 lines 205-209: I am wondering whether the typical vertical wavelength of 3km which is emphasized by this composite means something.

Author Response: We are not quite sure. One thing comes to mind, which is that Alexander et al. (200) found that temperature fields are dominated by waves of vertical wavelengths ~ 2 km, which is not so different than 3 km. However their result is for the tropical lower stratosphere 18 – 25 km so their findings may not have a direct connection to the ~ 3 km structure we found.

Manuscript Changes: No changes made.

P13 line 266: The confinement hypothesized in P18 can only occur in Phase 1 (see their Fig 2.), not in Phase 2

Author Response: We mentioned that ice can be found in Phase 2 based on P18's Figure 2 right panel, where for $RH_{ic}=0.63$ you can see a small portion of the ice within Phase 2. We reworded this sentence to clarify this.

Manuscript Changes: At line 271 of the new manuscript, the sentence is now "P18 suggests that (1) ice crystals within a confined range of r_e are suspended in Phase 1, and (2) for low background relative humidity with respect to ice (RH_{ib}), the confinement in Phase 1 may be positioned closer to Phase 2."

P13 line 270: Note that P18 derivation is also valid for a constant background wind (the exact same set of equations are obtained considering a frame moving at the constant background wind speed). However, it is true that the background wind shear cannot be as easily included in their approach and is neglected.

Manuscript changes: This sentence (now at line 274 of the revised manuscript) is changed to note that only wind shear is neglected in P18.

P13 line 280 : A prediction of P18 is that the fall speed is comparable to the GW vertical phase

speed. To get an idea, could you compare the fall speed of a crystal (assumed spherical for simplicity) of that radius to the typical GW vertical phase speed in Fig. 6?

Author Response: Assuming a radius of 15 μm and temperature of 200 K, P18's equation (20) (valid for radii of 5-100 μm) yields a sedimentation velocity of $\sim 2\text{cm/s}$. This corresponds to a displacement of $\sim 1.3\text{ km}$ over 18 hours. In Figure 6, using the cold anomaly in -12 to +6 hours, the descent rate is about 1 km, which is comparable to the ice sedimentation velocity.

Manuscript Changes: A paragraph is added at line 221 to describe P18's prediction regarding the fall speed, and how the descent rate of the cold anomaly rates to the estimated ice fall speed.

P15 line 285: Again, P18-type confinement always occurs in phase 1 for a monochromatic wave. With lower R_{hic} , the location gets closer to the boundary between phase 1 and 2, so that with a superposition of waves both phases might show similar cloud fraction.

Manuscript Changes: Sentence at line 290 is modified to say that in low R_{hic} ice gets closer to Phase 2 (instead of being inside Phase 2).

P 15 lines 290-300: It is an interesting approach that the authors attempt here, and I like the new Fig 11 in the reply to referee 1. However, I see small issues with the method employed by the authors.

First, the non-linearity of the Goff-Gratch equation means that the coarse resolution MLS water vapor divided by the saturation pressure of the mean temperature will lead to a larger relative humidity than the average relative humidity (average ratio of the two). This might explain why the authors estimates seem slightly high-biased compared with in situ observations of TTL humidity (see for instance Jensen et al., 2017 for a survey of TTL relative humidity from in situ measurements). This might result in a systematic bias in the authors' estimate. However, I imagine that the trend found by the authors will not be not sensitive to this.

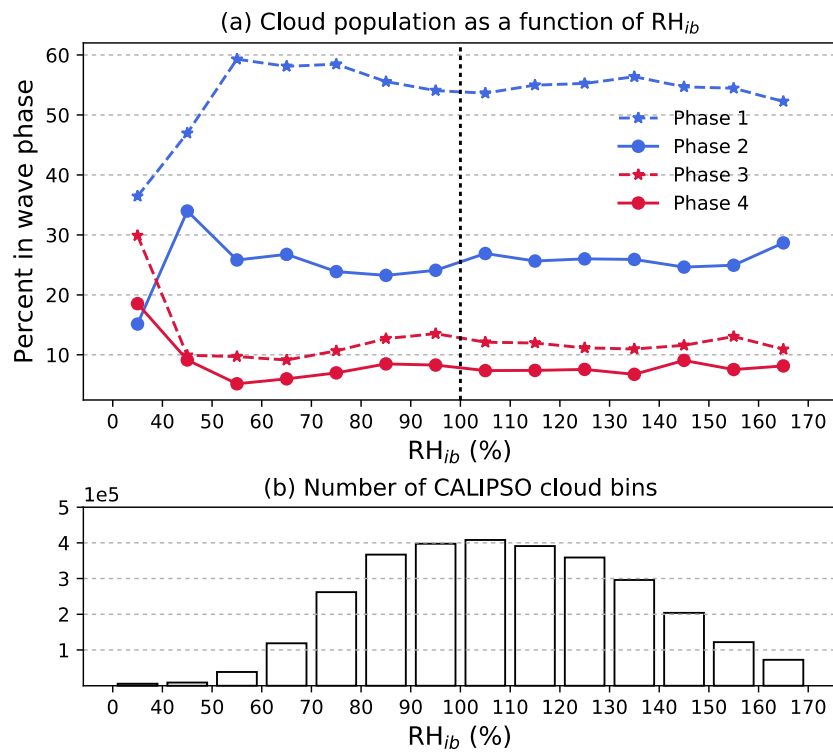
Second, as far as I understand, the temperature is estimated from 7-day averages but the water vapor from instantaneous values. For consistency, the water vapor should be taken from averages as well.

Author Response:

We will note in the text that the coarse resolution of the MLS and the nature of the Goff-Gratch equation may have contributed to the high-biased RH estimates. Regarding your second point, we have tried to calculate Figure 11 with 7-day averages of moisture, as shown below. In this Figure, the Phase 1 fraction increases up to $\text{RH} = 60\%$, and then there isn't much dependence on RH after that. However, the number of samples below 60% is very small.

We tend to think that the previous approach (using 7-day temperature but instantaneous mixing ratio) makes more sense physically. The goal is to use a "background" temperature that is unperturbed by the wave, and it is assumed that the 7-day temperature represent this temperature. Aside from wave anomalies, the basic state of temperature wouldn't vary much over 7 days (in the tropics), so this assumption is probably adequate. For "background" moisture,

ideally we'd be able to get the mixing ratio just before the wave passes through. However, unlike temperature, moisture can vary in short timescales (i.e. due to processes such as convection), so the 7-day average moisture is likely to be biased low compared to the actual background moisture. Because of this, we think that using the time-located MLS mixing ratio is a better way to find the relationship between RH_{ib} and clouds, although it is by no means ideal. For this reason, we are inclined to keep the previous approach.



Manuscript Changes: At line 305, we added a short discussion on why our RH estimates are high-biased.

P16 line 343: 4-5 km seems larger than the typical wavelength which comes out of your composites Fig. 6

Manuscript changes: We have rewritten this part to be clearer about what we wanted to convey. The new addition is: “The vertical wavelength inferred from the anomalies in our composites is about 3 km. Dzambo et al. (2019) showed that the power spectrum of TTL gravity waves tend to peak at wavelengths of around 4--5 km, though at 3 km there is still considerable power (their Figure 1). These wavelengths are all resolvable by RO, so it can be assumed that this analysis has included a large part of the TTL gravity wave spectrum.”

P16 lines 345-348: “Since negative dT_0/dz corresponds to a positive cooling rate (due to downward phase propagation as explained by K16), weakened stability, as well as upward vertical motion wave anomalies (according to the gravity wave polarization relationships),”: the two points “positive cooling rate” and “upward vertical motion” are equivalent under the usual adiabatic

approximation. One should be removed from the sentence

Manuscript Changes: “positive cooling rate” has been removed here.

Wording

P1, line 20: Maybe replace “favor” by “is favorable to” or use a passive.

Manuscript Changes: “favor” changed to “is favorable to”

p7 line 167: ‘vertical cloud fraction’: I would remove vertical.

Manuscript Changes: “vertical” has been removed

P7 line 168: ‘cloud boundaries’ → ‘cloud layer’ ?

Manuscript Changes: “boundaries” changed to “layer”

P7 line 175: Again, I would put a passive form.

Manuscript Changes: This paragraph has been rewritten in response to Referee 1’s comments, so the word “favor” is no longer there.

P10 line 213 : “a similar compositing technique ...” → “a compositing technique similar to the one employed above “

Manuscript Changes: Changed as suggested

P16 l340 : large wavelengths→large horizontal wavelengths

Manuscript Changes: Changed as suggested

References

Alexander et al., (2001): Gravity waves in the tropical lower stratosphere: A model study of seasonal and interannual variability, JGR-atmospheres.

Influence of gravity wave temperature ~~anomaly~~ anomalies and ~~its~~ their vertical ~~gradient~~ gradients on cirrus clouds in the tropical tropopause layer – a satellite-based view

Kai-Wei Chang¹ and Tristan L'Ecuyer²

¹Department of Atmospheric Sciences, Texas A&M University, College Station, Texas, USA

²Department of Atmospheric and Oceanic Sciences, University of Wisconsin-Madison, Madison, Wisconsin, USA

Correspondence: Kai-Wei Chang (kchang37@wisc.edu)

Abstract.

Negative temperature perturbations (T') from gravity waves are known to ~~favor~~ be favorable to tropical tropopause layer (TTL) clouds, and recent studies have further suggested a possible role of dT'/dz on facilitating TTL cloud formation and maintenance. With a focus on exploring the influence of dT'/dz on TTL clouds, this study utilizes radio occultation temperature retrievals and cloud ~~detection layers~~ from the Cloud-Aerosol Lidar and Infrared Pathfinder Satellite Observations (CALIPSO) to understand how gravity wave perturbations modulate cloud occurrence in the tropics.

Cloud populations were evaluated in four phases corresponding to positive or negative T' and dT'/dz . We find that ~~57.55%~~ 57.55% of TTL clouds are found where T' and dT'/dz are both negative. Regions of frequent convection are associated with higher cloud populations in the warm phase $T' > 0$. ~~The~~ We show that the partitioning of cloud population among wave phases ~~shows~~ some dependence on the ~~exhibit dependence on~~ background relative humidity ~~estimated using Aura Microwave Limb Sounder water vapor retrievals. Using effective radius (r_e) retrievals from the CloudSat/CALIPSO 2C-ICE product, we find that r_e is distributed similarly among all wave phases but a smaller mode is found in the r_e distribution from the phase $T' < 0$. In the phase where T' and $dT'/dz < 0$~~ dT'/dz are both negative, the mean cloud effective radius is the smallest of all four phases, but the differences are small.

It is shown that the strongest mean negative T' anomaly is centered on the cloud top, resulting in positive dT'/dz above the cloud top and negative dT'/dz below. This negative T' anomaly propagates downward with time ~~consistent with~~ characteristic of upward propagating gravity waves. Negative (positive) T' anomalies are associated with increased (decreased) probability of being occupied by clouds. The magnitude of T' correlates with the increase or decrease in cloud occurrence, giving evidence that the wave amplitude influences the probability of cloud occurrence. While the decrease of cloud occurrence in the warm phase is centered on the altitude of T' maxima, we show that the increase of cloud occurrence around T' minima occurs below the minima in height, indicating that cloud formation or maintenance is facilitated mainly inside negative dT'/dz . Together with existing studies, our results suggest that the cold phase of gravity waves ~~favor~~ is favorable to TTL clouds mainly through the region ~~of wave anomalies~~ where dT'/dz is negative.

25 **1 Introduction**

Variations in stratospheric water vapor (SWV) influence the rate of surface warming due to climate change (Solomon et al., 2010) and have a significant climate feedback (Banerjee et al., 2019). There is a need to better understand mechanisms controlling the amount of SWV, as they are potentially key components of climate change and stratosphere-troposphere coupling. Since the large-scale slow upwelling throughout the tropical tropopause layer (TTL) brings air from the troposphere into the lower stratosphere, conditions and processes in the TTL modulate the amount of water vapor in the lower tropical stratosphere. Cirrus formation by cold temperatures in the TTL is generally regarded as the primary mechanism dehydrating air entering the stratosphere (Holton et al., 1995). Studies have shown that cirrus cloud occurrence strongly associates with Kelvin waves (Immler et al., 2007; Fujiwara et al., 2009) and gravity waves (Suzuki et al., 2013; Kim et al., 2016), and that these waves can enhance the dehydration occurring inside the TTL (Schoeberl et al., 2015).

35 Previous studies on waves and cirrus clouds generally show that enhanced cirrus cloud occurrence tend to coincide with the gravity wave phases with negative temperature anomalies. Through aircraft observations of the NASA Airborne Tropical TRopopause EXperiment (ATTREX) campaign (Jensen et al., 2013), Kim et al. (2016) (K16 hereafter) show that ice was found most frequently where the temperature anomaly (T') and vertical ~~slope~~ gradient of temperature anomalies (dT'/dz) were both negative, bringing the latter quantity into attention as a possible control on cirrus formation. Since K16 showed that the occurrence of convectively-coupled clouds had no preference towards the sign of T' or dT'/dz , the tendency of TTL clouds to ~~occur~~ exist in negative T' and dT'/dz likely depicts a connection between clouds and gravity wave perturbations. They suggest that the negative rate of change in temperature (positive cooling rate) in regions where $dT'/dz < 0$, due to the downward phase propagation of gravity waves, may facilitate cloud formation and explain the abundance of cloud in the phase with $T' < 0$ and $dT'/dz < 0$. Another explanation of high cloud frequency in this phase is given by Podglajen et al. (2018) (P18 hereafter) who used a simplified set of equations to model the interaction between ice crystal growth, sedimentation, and gravity wave perturbations of temperature and vertical motion. P18 argues that in this phase the upward vertical motion acts in concert with the sedimentation rate of ice crystals with certain sizes, suspending crystals inside this wave phase as it descends with the downward phase propagation of the wave. Since $dT'/dz < 0$ corresponds to a upward vertical wind anomaly, this result supports the presence of ice in negative T' and dT'/dz . Motivated by these studies, we aim to further explore this connection between gravity waves and cirrus clouds through satellite datasets.

This study utilizes temperature profiles from the radio occultation (RO) technique (Kursinski et al., 1997) which has been widely used to study equatorial gravity and Kelvin waves (Randel and Wu, 2005; Alexander et al., 2008; Scherllin-Pirscher et al., 2017). We collocate these RO profiles to cirrus cloud observations from the Cloud-Aerosol Lidar and Infrared Pathfinder Satellite Observations (Winker et al., 2010) to study the relationship between gravity/Kelvin wave phases and cirrus occurrence. Especially within ~~2006 to 2014~~ 2007 to 2013 there is a high spatial and temporal density of RO soundings from the U.S.-

Taiwan joint mission Constellation Observing System for Meteorology, Ionosphere, and Climate (COSMIC) (Anthes et al., 2008), allowing a large number of RO profiles to be collocated with cirrus cloud retrievals.

Collocations that are temporally close in time are used to evaluate wave perturbations T' and dT'/dz in relation to cloud occurrence and properties. In addition, since the sampling of COSMIC is pseudo-random in both space and time, it is possible to obtain RO profiles that are spatially close to CALIPSO footprints but before or after the time of the footprint. Using collocations of various time separations we build composite time series of wave anomalies and cloud frequency to understand how waves are influencing TTL clouds. Finally, we use the Aura Microwave Limb Sounder (MLS) water vapor retrievals (Read et al., 2007) and ice cloud effective radius (r_e) retrievals from the CloudSat/CALIPSO 2C-ICE product (Deng et al., 2013, 2015) to evaluate whether relative humidity and r_e ~~have connections~~ are related to gravity waves as shown by P18.

Section 2 describes the datasets used in this study. In Section 3 we explain the extraction of wave temperature anomalies from RO profiles and the method for data collocation. In Section 4, results are given in three parts: Section 4.1 discusses the population of clouds in each wave phase, Section 4.2 presents the composite time evolution of wave anomalies and cloud frequency, and Section 4.3 evaluates the predictions of P18 with satellite observations. Our conclusions are summarized in Section 5.

2 Satellite products

This study uses the re-processed radio occultation (RO) atmPrf dataset processed by the Cosmic Data Analysis and Archive Center (CDAAC). We use occultations from the following satellite missions: Constellation Observation System for Meteorology, Ionosphere, and Climate (COSMIC) (Anthes et al., 2008), Meteorological Operational Polar Satellite A/Global Navigation Satellite System Receiver for Atmospheric Sounding (Metop-A/GRAS) (Von Engelmann et al., 2009), Metop-B/GRAS, and the Challenging Minisatellite Payload (CHAMP) (Wickert et al., 2001). Because the RO technique does not suffer from inter-satellite calibration effects (Foelsche et al., 2011), profiles from different satellite missions can be used together as long as they are processed with the same algorithm. The level 2 atmPrf dataset provides 'dry' profiles of atmospheric temperature derived by neglecting moisture, which is appropriate for TTL altitudes. The atmPrf provides temperature estimates at 30-meter vertical spacing, but the effective resolution of RO is around 200 meters in the tropical tropopause layer (Zeng et al., 2019). The precision of temperature is approximately 0.5 K within 8 to 20 km (Anthes et al., 2008).

The Cloud-Aerosol Lidar and Infrared Pathfinder Satellite Observations (CALIPSO) (Winker et al., 2010) is a sun-synchronous, polar-orbiting satellite along the NASA A-Train formation, ~~overpassing~~ passing the equator at 0130 and 1330 local solar time. Its primary instrument, the Cloud-Aerosol Lidar with Orthogonal Polarization (CALIOP), is a dual-wavelength lidar capable of detecting subvisual clouds with optical depths less than 0.01. We use the Level 2 V4.10 5-km Cloud Layer product for estimates of cloud top and base altitude and the V4.10 5-km Cloud Profile product for detection of clouds in 60-meter vertical bins. The Cloud Aerosol Discrimination (CAD) ~~Score~~ score in these products is a measure of confidence that the detected feature is correctly classified as cloud. To ensure high confidence that all analyzed features are clouds, our analysis only includes CALIPSO layers and bins with CAD score ~~at or above~~ of 80 or higher (where 100 means complete confidence in the feature).

being a cloud). Corresponding to the dates when RO data were available, we use nighttime CALIPSO data between ~~2006 and 2014~~, 2007 and 2013. Daytime CALIPSO data were excluded due to the lower signal-to-noise ratio of daytime CALIOP observations.

Estimates of ice cloud effective radius (r_e) come from the 2C-ICE product (Deng et al., 2013, 2015) which is derived jointly using the CloudSat radar and CALIPSO lidar observations. This product provides r_e retrievals at 1-km footprints in 250-m vertical bins. The r_e estimates from 2C-ICE compare well to in-situ flight measurements with a mean retrieval-to-flight ratio of 1.05 (Deng et al., 2013). For quality control, we only use r_e with uncertainty (given by the `re_uncertainty` variable) less than 20%. Due to a battery failure CloudSat left the A-Train formation in 2011. After that it only operated in daytime and its footprint was no longer collocated to CALIPSO. For this reason we limit our analysis ~~to using~~ 2C-ICE ~~from to~~ 2007 to 2010 when nighttime data was available.

The Aura MLS H₂O product provides retrievals of water vapor mixing ratio at pressures at and below 316 hPa with a precision of 0.2-0.3 ppmv (4-9%) in the stratosphere (Lambert et al., 2007). We use the water vapor mixing ratio to estimate relative humidity with respect to ice (RH_i) using collocated RO temperature. Criteria for data screening follows all the recommendations outlined in section 3.9 of the ~~official documentation (Livesey et al., 2017)~~ found at product documentation (Livesey et al., 2017). Although Aura was launched in 2004, the scan of the MLS did not align with that of CALIOP until May 2008. For this reason, all analysis involving this product ~~uses data from~~ is limited to 2008 to ~~2014-2013~~.

105 3 Methods

3.1 Gravity wave temperature anomalies

Our method for obtaining temperature perturbations (T') due to gravity waves is based on Alexander et al. (2008). Mean temperature profiles are calculated on grid boxes of 20° longitude × 5° latitude × 7 days centered on each day of year. Mean maps are made for each day between 1 ~~Nov 2006 and 30 April 2014~~ Jan 2007 and 31 December 2013 during which COSMIC provided a large number of RO observations. For an arbitrary RO temperature profile, the mean map centered on the same day as the RO profile is used to derive the corresponding mean-state profile through bilinear interpolation of the four grid boxes surrounding the location of the given RO profile. T' is then obtained by removing the ~~mean-state~~ mean state from the actual profile. Since we use a 7-day mean state, the resulting T' can be thought of as representing variability on timescales less than seven days. After T' is obtained, its vertical gradient is calculated to get dT'/dz . Figure ~~??~~ 1 shows one example of a temperature profile, its corresponding mean state, and the resulting anomalies T' and dT'/dz .

3.2 Collocation of CALIPSO observations to RO profiles

The primary goal of this work is to study cirrus occurrence and properties in the four gravity wave phases defined in Figure ~~??~~ 1. To accomplish this we collocate CALIPSO cloud observations to RO temperature profiles. The horizontal weighting of RO retrievals is mostly centered within 200 to 300 km of the perigee (tangent) point (Kursinski et al., 1997) where the ray

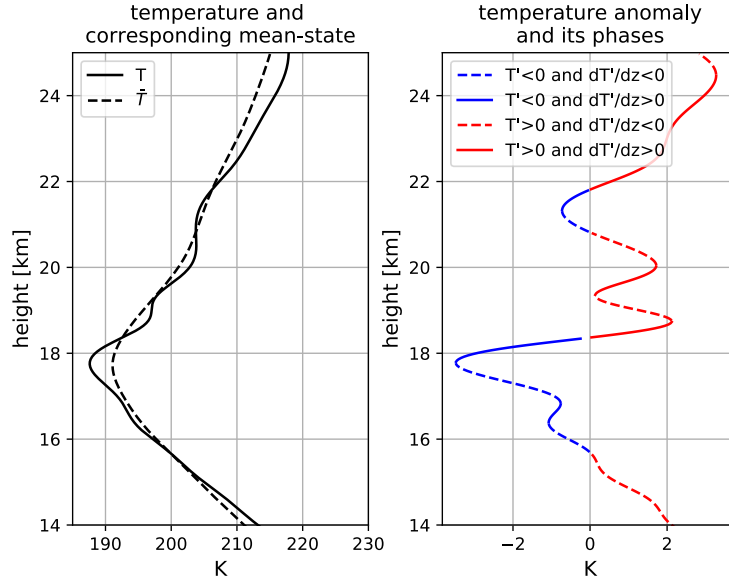


Figure 1. (Left) Temperature profile (solid line) from COSMIC at $155^{\circ} 43' \text{ W}$, $18^{\circ} 16' \text{ N}$ on 1 Jan 2007 and its corresponding mean-state (dashed). (Right) T' of the given profile and its four phases based on the sign of T' and dT'/dz .

120 experiences most bending. For this reason we use the spatial location of the perigee point as basis for collocation. Since our interest lies strictly inside the TTL and the perigee point of each occultation ray changes with height, we determine the perigee point at the middle of the TTL by interpolating the longitude and latitude of RO profiles to 17.25 km (middle of TTL determined as the average of 14.5 km and 20 km). Any CALIPSO observations within 100 km of this point are collocated to the RO profile for analysis. ~~Collocation radii of 50 and 200 km were also tested, and we found that the results were similar to the choice of~~
 125 ~~100 km.~~ [Figure ??](#) [Figure 2](#) gives an example of one RO profile, its perigee point at 17.25 km, and the collocated CALIPSO 5-km footprints.

We collocate RO profiles to 2C-ICE cloud retrievals in a similar manner. Unlike the CALIPSO 5-km products, 2C-ICE provides cloud properties at 1-km footprints and vertical bins of approximately 250 m. Other than this difference, the collocation method is identical to that of CALIPSO and RO. In May 2008 the Aura MLS was aligned to within ± 10 km of CALIOP.
 130 For analysis involving RH_i , for each CALIPSO footprint with a RO collocation, we find the closest MLS footprint to that CALIPSO footprint to calculate RH_i .

4 Results

All results below were derived from data within 20° of the equator. For convenience we will refer ~~the the to the~~ [the four](#) gravity wave phases as follows. Phase 1: $T' < 0$ and $dT'/dz < 0$; [Phase 2: \$T' < 0\$ and \$dT'/dz > 0\$](#) ; [Phase 3: \$T' > 0\$ and \$dT'/dz < 0\$](#) ; [and Phase 4: \$T' > 0\$ and \$dT'/dz > 0\$](#) . Cold and warm phases refer to where $T' < 0$ and $T' > 0$, respectively.

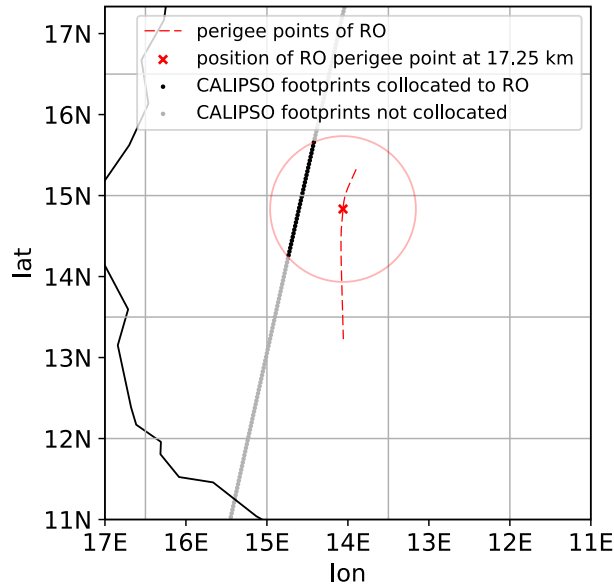


Figure 2. Schematic of collocation between RO profile and CALIPSO footprints. The perigee points of the RO profile throughout all altitudes are shown in the red dashed line, while the position of the perigee point in the middle of the TTL (17.25 km) is denoted by the red X. The CALIPSO 5-km product provides estimates of cloud properties at 5-km footprints, and all footprints within 100 km of the red X are collocated with the RO profile, as indicated by the black dots. Gray dots are CALIPSO footprints are considered too far from the RO profile and not collocated. The shown RO profile was taken at approximately 0120UTC 2 Jan 2009.

For the analysis presented in Section 4.1 and Section 4.3, the temporal restriction for collocation is that all the collocated data must be within two hours of each other. This restriction is not imposed in 4.2, and the time difference between RO and CALIPSO observations range from 0 to 36 hours with the purpose of examining how waves and cirrus clouds tend to evolve over time. This will be further elaborated in that section.

140 4.1 Population of clouds in wave phases

As previously mentioned, K16 (their Figure 5) found that a majority of TTL clouds in the ATTREX data were observed in the cold phase $T' < 0$ and that in the 2014 flight legs over the Western Pacific there was a higher frequency of ice inside $dT'/dz < 0$ than in $dT'/dz > 0$. To assess whether this tendency is general throughout the TTL or is limited to the regions observed by ATTREX, we evaluate cloud populations using collocated CALIPSO and RO observations that cover the TTL at all longitudes and over ~~2007–2014~~. ~~Figure ??~~ ~~2007–2013~~. ~~Figure 3~~ shows the population of CALIPSO Cloud Profile vertical bins detected as clouds in each wave phase extracted from collocated RO profiles. Considering all collocated observations between ~~1 Nov 2006 and 30 April 2014~~, ~~57~~ ~~January 2007 and 31 December 2013~~, ~~54.9%~~ of clouds are observed to occur in Phase 1 throughout the entire TTL, as shown in Figure ~~??~~3(a). When the cloud population is examined in 1-km vertical layers

(14.5–15.5 km, 15.5–16.5 km, etc.), there is no obvious change with height and most clouds are found in Phase 1 followed by
150 Phase 2 at all heights. Above 16.5 km there is a smaller fraction of clouds in the warm phase. A possible explanation for this
may be that there are less convectively detrained clouds as altitude increases, increasing the probability of clouds having been
formed by gravity waves. In addition, the population in Phase 2 tends to increase with height, with 38% of clouds above 17.5
km in Phase 2. For comparison, using K16's Figure 5 one can infer that for clouds above 16.5 km the cloud fraction in Phase
1, 2, 3, and 4 are 56.25%, 31.25%, 9.375%, and 3.125% (calculated as the percentage in that phase divided by the sum all four
155 phases), and for clouds below 16 km the percentages are 49.30%, 28.17%, 14.08%, and 8.45%. These ratios are similar to our
findings, though we find less clouds in Phase 2 below 16 km. While the percentages in Figure 3(a) are representative of the
entire tropics, the above estimates based on K16's Figure 5 are based on observations over the Western Pacific. We split the
tropics into smaller regions to facilitate better comparison.

Cloud fractions in each phase are separated into six longitudinal belts in Figure ??-4. Filled bars represent the cloud
160 fraction of all TTL clouds while unfilled bars represent only clouds above the mean tropopause of their respective season and
longitudinal belt. During December-January-February (DJF), the 120°E-180°E belt, which covers the Maritime Continent and
Western Pacific, has the lowest cloud population in Phase 1 (~~52~~51%) as well as the most clouds inside the warm phase (24%).
Although this region is known for very low tropopause temperatures and high TTL cirrus frequency during ~~boreal-winter-DJF~~
(Highwood and Hoskins, 1998; Sassen et al., 2009), there is also frequent deep convection (Ramage, 1968) which may generate
165 clouds unrelated to gravity waves. This may explain the higher cloud population in warm phases. By eliminating clouds below
the tropopause, above which convective detrainment is rare, the amount of clouds inside the warm phase in this region reduces
to 10%.

The influence of convection may also explain the high warm phase population during June-July-August (JJA) in 60°E-120°E
where there is frequent convection due to the Asian ~~Monsoon~~summer monsoon. In this period and region, 28% of clouds are
170 in the warm phase and 47% ~~is~~ are in Phase 1. However, the reduction of cloud population in the warm phase after eliminating
clouds below the tropopause is not as apparent here. One possible cause of this may be that the tropopause within 10°N to
40°N is elevated due to the Asian monsoon anticyclone in the upper troposphere, causing the tropopause to be more than 1 km
higher than the zonal mean (Ploeger et al., 2015). Since our mean tropopause is calculated based on all profiles within 20°N
to 20°S, some clouds from convective detrainment (especially those in the Northern Hemisphere) may still be included in the
175 cloud population.

Over 180°W-120°W, which approximately covers the Eastern Pacific, ~~62%~~(~~27~~56% (~~25~~%) of clouds fall in Phase 1 (Phase
2) during DJF. This is in contrast with K16 who found that in the 2011 and 2013 ATTREX flight legs over the Eastern Pacific
there were slightly more clouds in Phase 2 than in Phase 1. The 2011 flights were conducted in October and November while
the 2013 flights were in February and March. Plots similar to Figure ??-4 made from data in October-November (not shown)
180 yielded Phase 1/2 populations of ~~63~~64%/~~24~~23% while February-March yielded ~~58~~57%/20%. Over this region we were not
able to find Phase 2 having more clouds as K16 did. ~~It is not clear what causes this difference.~~ Their T' were calculated as
the difference between aircraft in-situ temperature and 30-day mean temperature derived from RO, while we calculate it as the
difference between RO-derived temperatures and 7-day mean profiles. ~~This difference in methodology may be a factor causing~~

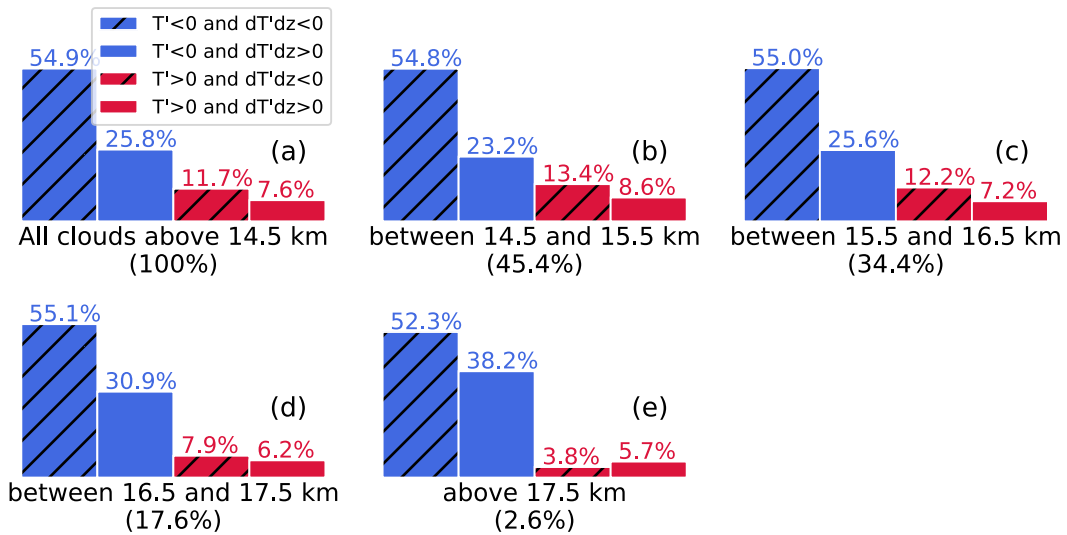


Figure 3. Population of CALIPSO Cloud Profile cloud bins inside each wave phase from 1 [November 2006–January 2007](#) to [30 April 2014–31 December 2013](#). Plot (a) shows the cloud [fraction–population](#) for all of TTL (14.5 to 20 km), while (b)–(e) show the population in three different 1-km layers. The percentage in parenthesis denote the portion of clouds found in that vertical layer relative to all TTL clouds.

185 [the contrasting findings–Reproducing the cloud population using 31-day mean temperature as the background still resulted in more clouds in Phase 1 than 2 \(not shown\). It is not clear what causes this difference.](#)

Using the cloud top and base heights reported from the CALIPSO Cloud Layer product we calculate the [vertical–cloud fraction](#) in each wave phase, defined as the amount of vertical overlap between [the cloud boundaries and the line segments in Figure ?? corresponding to each phase](#). [The distributions of vertical–individual cloud layers and wave phases in Figure 1.](#) For example, if a phase layer occupies 15.0 to 16.0 km and the CALIPSO product reports a cloud layer extending from 15.2 to 15.7 km, then the cloud fraction would be 0.5. [The cloud fraction of each observed wave phase is evaluated, and the resulting distributions of cloud fraction are shown in Figure ?? \(for cloud fractions between 0 and 1\) and Table ?? \(for cloud fractions equal to 0 and 1\).](#) In this figure and table we only consider clouds with base above 14.5 km and wave phase [segments–layers](#) whose base height lie within 14.5 and 18.5 km. [Note that cloud fractions of 0 and 1 are excluded in this figure. Corresponding to Figure 5, the total sample number in each phase is shown in the first column of Table 1, while the number of cases with unity cloud fraction is shown in the second column.](#)

195 In phases of positive dT'/dz , the number of samples tend to decrease as cloud fraction increases. This trend doesn't apply for negative dT'/dz , and in Phase 1 there is a clear increase of samples with increasing cloud fraction. [Phase 1 also has the most cases where the vertical cloud fraction is unity \(19410 cases\).](#) Overall, Phase 1 is most distinct as it has most samples with cloud fractions of unity and it significantly favors higher values of vertical cloud fraction. [In contrast, Phase 2 and 4 tends to have smaller cloud fractions, while Phase 3 has a rather uniform distribution across all values. It is interesting that Phase 3](#)

200

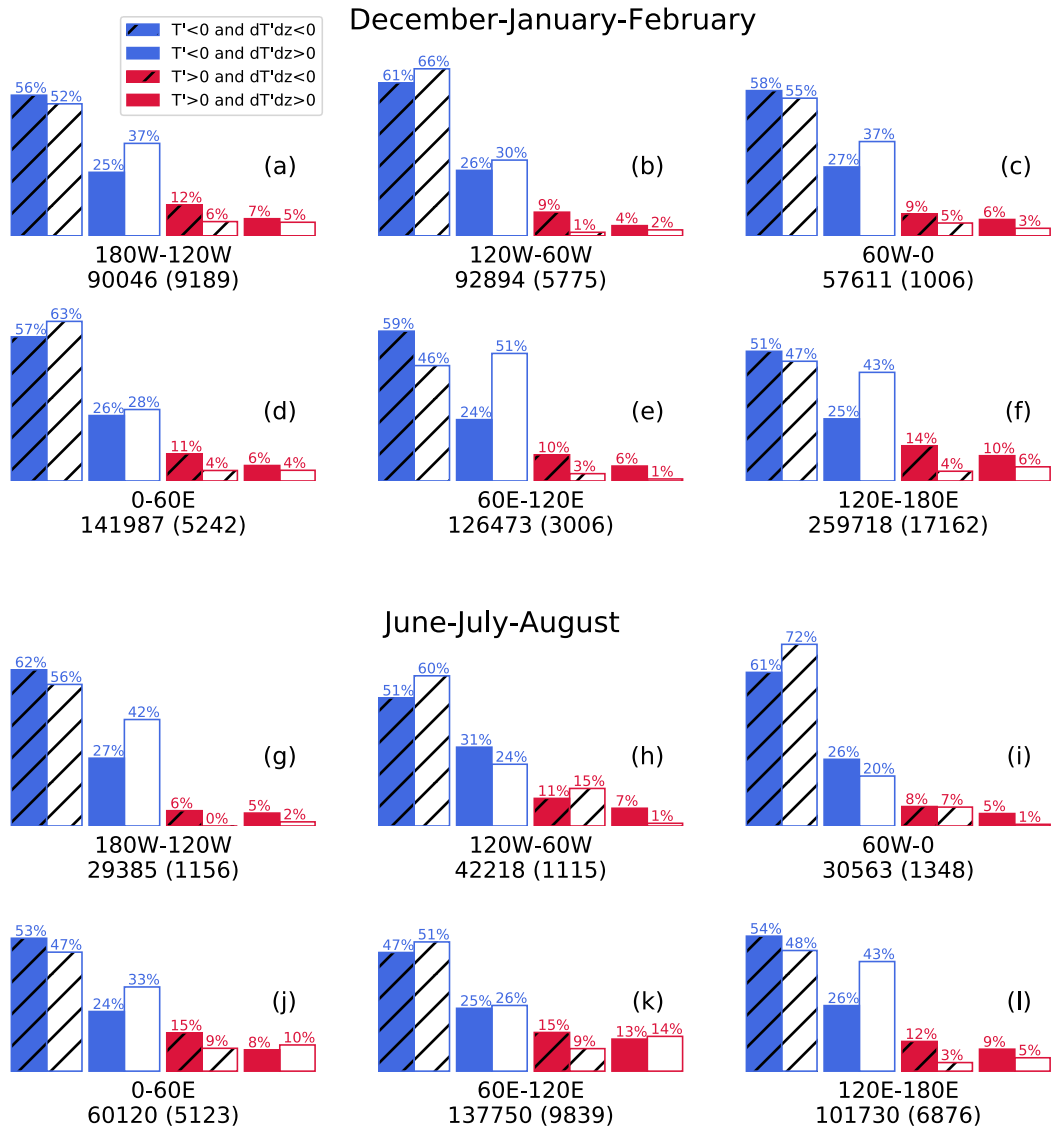


Figure 4. Same as Figure ??(a) except for different longitudinal belts. Plots (a)-(f) are for December-January-February and (g)-(l) are for June-July-August. Filled bars represent all TTL clouds, while unfilled bars represent only clouds above the mean tropopause of the respective longitudinal belt and season. The numbers of all cloud bins and bins above the tropopause (in parenthesis) in each longitudinal belt are labeled under each bar plot.

has high percentage (43%) of unity cloud fraction, much higher than Phase 4. Although both Phase 3 and 4 both have positive temperature anomaly, we find that Phase 3 seems to be much more favorable for clouds, consistent with P16's assertion that upward vertical wind anomaly is an important factor in maintaining ice clouds.

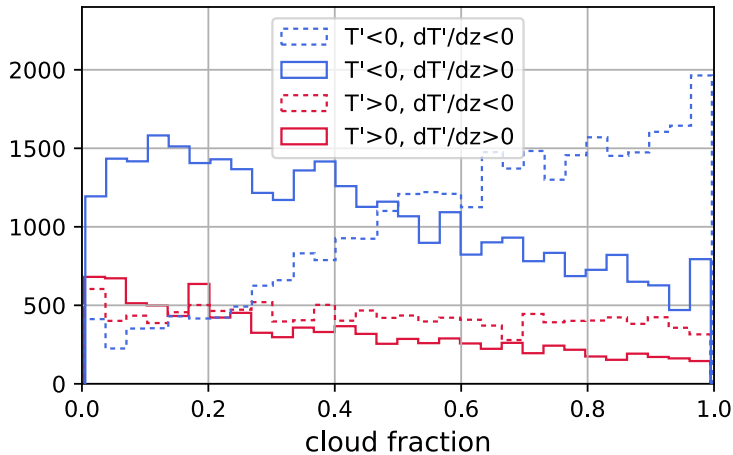


Figure 5. Distribution of ~~vertical~~-cloud fraction in each gravity wave phase. Blue and red colored lines indicate the cold and warm phase, respectively, while the solid and dashed lines represent $dT'/dz > 0$ and $dT'/dz < 0$. The number of cases with ~~vertical~~-cloud fractions of zero or unity are ~~not plotted in this figure and is instead shown in Table ??excluded~~.

Table 1. Number of cases with ~~zero or unity vertical~~-cloud fraction (CF) between 0 and 1 (sum of cases in Figure 5), and CF = 1. The percentage represents the number of CF=1 cases over the sum of the respective row.

Wave Phase	CF=0 <u>CF=0<CF<1</u>	CF=1
Phase 1	432,838 <u>30,519</u>	19,410 (<u>38.9%</u>)
Phase 2	461,251 <u>32,152</u>	10,656 (<u>24.9%</u>)
Phase 3	441,906 <u>12,687</u>	9,583 (<u>43.0%</u>)
Phase 4	457,166 <u>9,784</u>	999 (<u>9.3%</u>)

4.2 Composite time evolution of wave anomalies and cirrus occurrence

205 Since COSMIC observations are pseudo-random in time and space, it is possible to collocate CALIPSO observations to RO
soundings with varying offsets in time. By binning the temperature profiles according to the time offsets, we can make a
composite showing the mean time evolution of wave anomalies relative to the cloud observation. Such an approach of creating
composite time series has been used to study the thermodynamic budget before and after tropical convection (Masunaga, 2012;
Masunaga and L'Ecuyer, 2014), temperature anomalies associated with tropical deep convection (Paulik and Birner, 2012),
210 and the interaction between atmospheric dust and tropical convection (Sauter et al., 2019).

We bin RO profiles in time bins of $-35, -33, \dots, -1, 1, \dots, 33, 35$ hours relative to the CALIPSO observations, where a
negative value indicates that the collocated RO profiles precede the CALIPSO overpass. The composites of T' , dT'/dz , and
buoyancy frequency N^2 anomaly for all collocations in ~~2006 to 2014~~2007 to 2013 are shown in Figure ~~??6~~. In making these
composites we only includes clouds with cloud base of at least 14.5 km to ensure that the included clouds are TTL clouds

215 (instead of, for example, convection) Also, for statistical testing, we need the RO profiles used in each time bin to be unique. For this reason, only the CALIPSO footprint spatially closest to the RO profile is used. If this is not done, then the same RO profile may be reused several times since there are usually multiple CALIPSO footprints collocated to one RO profile as shown in Figure ???.

In Figure ??6(a), the strongest cold anomaly is found close to the cloud top and is coldest near hour 0. The cold anomaly contour with value below -0.6 -0.8 K lasts approximately from -15 -12 to +6 hours, and migrates downward with time consistent with the property of gravity and Kelvin waves with upward group velocity. The alternating cold-warm anomaly at heights of 2 to 6 km should be due to the diurnal tide (Zeng et al., 2008; Pirscher et al., 2010) since we are compositing only on nighttime data from CALIPSO which always ~~overpasses~~ crosses the equatorial region at similar local times. The number of samples in each time bin (Figure ??(d6(c))) has a 12-hour periodicity mainly due to Metop-A/B. When only using COSMIC observations to ~~make Figure ??~~ reproduce Figure 6(a), (b), and (d), the anomaly patterns are largely the same so the periodicity does not affect the composites.

It is noteworthy that the mean cold anomaly is centered near the cloud top and not within the cloud. This results in a dipole structure in dT'/dz (Figure ??6(b)) and buoyancy frequency anomaly (Figure ??6(d)) with positive anomalies just above the cloud top and negative anomalies below. This structure shows that the inside of clouds (below cloud top) is likely to have negative dT'/dz , consistent with the finding by K16 and Figure ??-3 that a majority of clouds are found in Phase 1. Although this structure implies weakened stability (negative N^2 anomaly) inside the cloud, it is unclear whether this decreased stability has connections to cloud formation or maintenance. Since negative dT'/dz also corresponds to upward vertical motion anomalies (assuming that these anomalies are from gravity waves), ~~further study is required to separate the role of vertical motion and stability in how gravity and Kelvin waves influence TTL clouds. their effects are difficult to separate.~~

235 A prediction of P18 is that the ice sedimentation velocity is comparable to the gravity wave vertical phase speed. In Figure 6, the descent rate of the cold anomaly within -12 to $+6$ hours is about 1 km over 18 hours. Assuming a spherical ice crystal with radius of $15 \mu\text{m}$ and ambient temperature of 200 K, P18's equation (20) (valid for radius in 5 - $100 \mu\text{m}$) yields a sedimentation velocity of $\sim 2\text{cm/s}$. This corresponds to a displacement of ~ 1.3 km over 18 hours, which is comparable to the vertical descent rate of the cold anomaly.

240 Figure ??-7 is similar to Figure ??-6 except the anomalies are not composited relative to the cloud top height but rather on height above mean sea level. In this composite, there are cold anomalies at TTL altitudes but the magnitude is weaker than that of Figure ??6. This leads to weak anomalies in dT'/dz (Figure ??7(b)) and N^2 (not shown). Based on these results we suggest that gravity wave anomalies in Figure ??-6 are physically significant and have a close association with the vertical position of TTL cloud tops.

245 P18 argues that the upward vertical velocity in Phase 1 slows down the descent of ice crystal and tends to suspend them inside Phase 1. Since these composites depicts a downward propagation of wave anomalies, it is of interest to investigate whether the phase propagation of gravity waves is associated with a downward migration of clouds. We can explore this possibility through a ~~similar compositing technique~~ compositing technique similar to the one employed above. Instead of centering on the CALIPSO footprint, we ~~centered~~ center on the time of RO sounding, and use the CALIPSO cloud product to calculate the

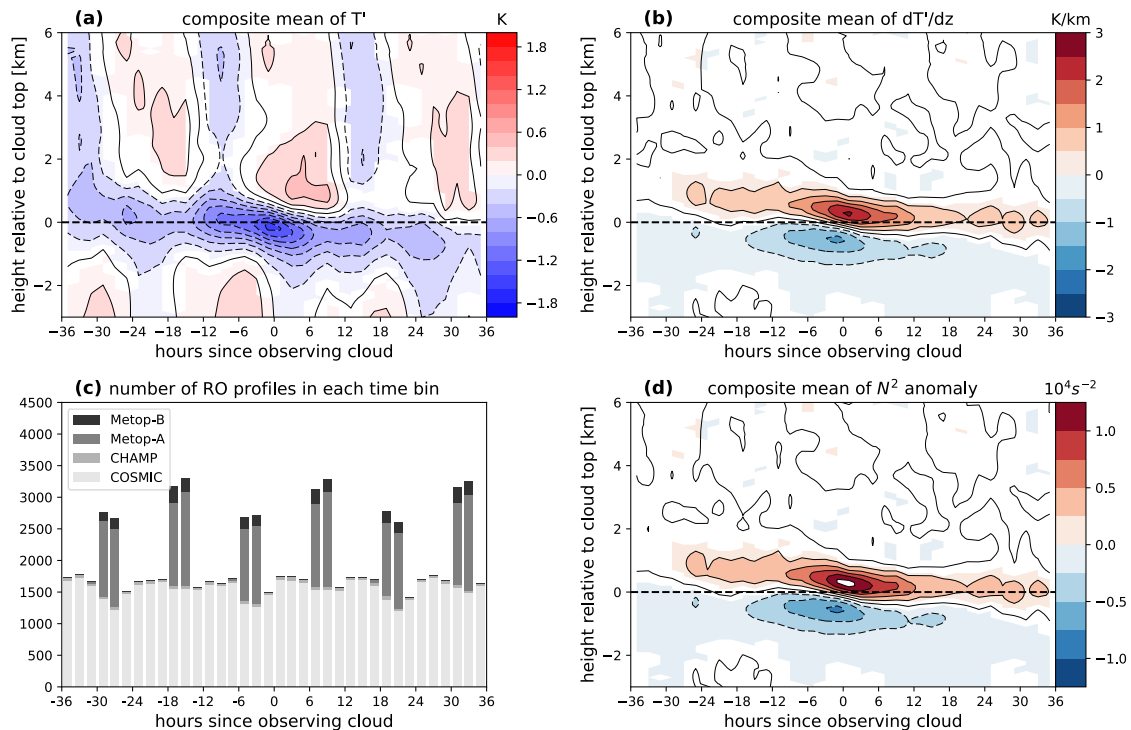


Figure 6. Composite of (a) T' , (b) dT'/dz , and (d) buoyancy frequency N^2 anomaly in height coordinate relative to cloud top. Colored contours in these three plots are at or above the 95% significance level according to the Student's t-test. Solid (dashed) contours represent positive (negative) anomalies and are at the same levels as the colored contours. The abscissa denotes the time offset between the CALIPSO observation and RO sounding. Plot (c) shows the number of unique RO profiles in each 2-hour time bin used to calculate the composites.

250 cloud frequency in each 2-hour time bin. In addition, instead of compositing relative to cloud top height, we composite on the altitude of the *local* minima or maxima of T' . A schematic of this compositing approach is given in Figure ???.

In the example shown in Figure ???(a), at day i there is a collocated RO sounding that occurred within 100 km of the CALIPSO footprint but Δt_i hours after. The position of the cloud top and base (solid and dashed magenta lines) is evaluated relative to a local T' minimum. Since the CALIPSO overpass occurred before this RO profile, in the compositing (shown in
 255 Figure ???(b)) the observed cloud position is used to calculate the cloud fraction at Δt_i hours *before* the RO sounding. The cloud fractions are calculated on a grid of 50-m height and 2-hour time bins. For the collocation pair in Figure ???(a), the cloud fraction in the time bin corresponding to $t = -\Delta t_i$ is calculated according to how much each vertical bin overlaps with the interval $[h_i^{(b)}, h_i^{(t)}]$. If the collocated CALIPSO footprint has no clouds with base above 14.5 km, cloud fractions of zero are still binned in the appropriate time bin at all heights. Since any RO profile most likely has multiple local minima, the binning
 260 of cloud fraction is repeated for each local minimum in a T' profile. The exact same procedure is conducted for local maxima to create a separate cloud frequency composite. To focus on TTL clouds we only include clouds with base at or above 14.5 km. Also, we only consider local T' extrema within 14.5 to 18.5 km since a majority of TTL clouds are inside this height range.

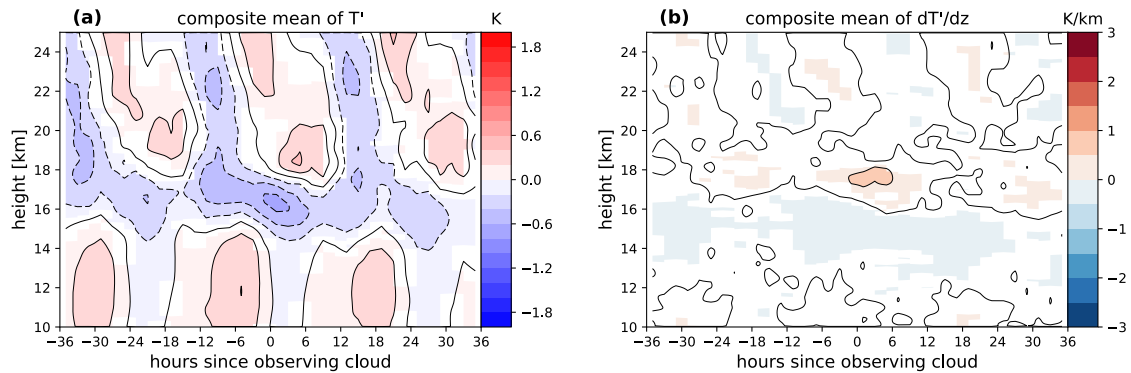


Figure 7. Same as Figure ?? Composites of (a) T' and ??(b) dT'/dz based on height above mean sea level (instead of height coordinate relative to cloud top as in Figure 6). Colored contours are at or above the 95% significance level according to the Student's t-test. Contour levels are identical to Figure ??6.

The composites of cloud frequency made this way, shown in Figure ??9(a)-(c) and (d)-(f), can then be interpreted as the probability of finding clouds in the vicinity of local T' minima or maxima, respectively. The shown values represent the mean cloud fraction in each time-height bin. Each column is produced from a different subset of T' extrema based on magnitude ($|T'| > 0.5, 1.0, \text{ or } 1.5 \text{ K}$). Beneath the vertical position of $\min(T')$ (Figure ??9(a)-(c)) we find a lobe of enhanced cloud frequency and this becomes more evident as $\min(T')$ decreases. Likewise, in the vicinity of $\max(T')$ (Figure ??9(d)-(f)) the cloud frequency is reduced, and this reduction also shows dependence on the magnitude of $\max(T')$. In both cases, the increased or decreased cloud frequency displays a downward trend consistent with the expectation that gravity wave phases propagate downward with time. However, it is hard to quantitatively know which parts of these plots are true anomalies. For this reason we We devise a way for extracting the anomalies in these patterns and for statistical testing, as described below.

The cloud frequency composites in the top two rows of Figure ?? are made using the altitude of the T' extrema as the zero height. To generate a composite where the vertical position of T' extrema has no relationship with cloud top/base height, for each T' extremum we generate a random altitude using uniform distribution $unif(14.5, 18.5)$ and make a separate cloud frequency time-height composite with the random altitude as zero height, shown in Figure ?? (to extract the cloud frequency anomaly associated with these patterns; the method and the statistical testing are detailed in the Appendix. To summarize the method briefly, we produce a background cloud frequency and compare it the pattern shows in Figure 9(a)-(i). These plots can be interpreted as the cloud frequency distribution one would expect if the vertical position of T' extrema has no connection to cloud top/base height. Then the statistically significant differences between the first/second row to the third row may signify a connection between wave anomalies and cloud occurrence. The distribution of cloud fraction in each time-height bin is similar to those shown in Figure ?? and therefore is not normal, so the Student's t-test cannot be used here. We use the two-sided two-sample c) and (d)-(f) to find statistically significant values through the Kolmogorov-Smirnov test (K-S test) (Hollander

et al., 2015) ~~which does not make any assumptions about the data distributions. This test can be used to evaluate whether two~~
285 ~~continuous or discrete probability distributions differ from each other. The K-S test is employed to compare the discrete cloud~~
~~fraction distribution in each time-height bin of the first/second row to the same bin in the third row. The null hypothesis is that~~
~~the first/second row is not different than the randomly-generated cloud frequency pattern in the third row.~~

~~The fourth row of Figure ?? (panels (j)-(l)) is the first row minus the third row, depicting the~~ Figure 9 are
the anomalies associated with $\min(T')$, and similarly ~~the fifth row (panels (m)-(o)) shows~~ l show the anomalies
290 associated with $\max(T')$. Colored portions of the contour denote regions with $p < 0.05$ (95% confidence) as estimated from
the K-S test. In these anomaly patterns it is confirmed that there is enhanced cloud occurrence below $\min(T')$, and, in addition,
a weak reduction of cloud occurrence above it. For the subset of $\min(T') < -0.5$, the positive cloud frequency anomaly peaks
at 3% whereas for $\min(T') < -1.5$ it peaks at 6%. The anomaly patters due to $\max(T')$ also exhibit a dipole structure with
negative anomalies centered on the altitude of $\max(T')$ and a weak positive anomaly below. ~~The fifth row~~ Panels (j)-(l) also
295 suggests a dependence of cloud frequency anomaly with respect to on the magnitude of $\max(T')$, although the variation is not
as large compared to that of $\min(T')$. Both positive/negative anomalies associated with $\min(T')$ / $\max(T')$ tend to migrate
downward in time, although this trend is slightly more apparent in the enhanced cloud occurrence of $\min(T')$.

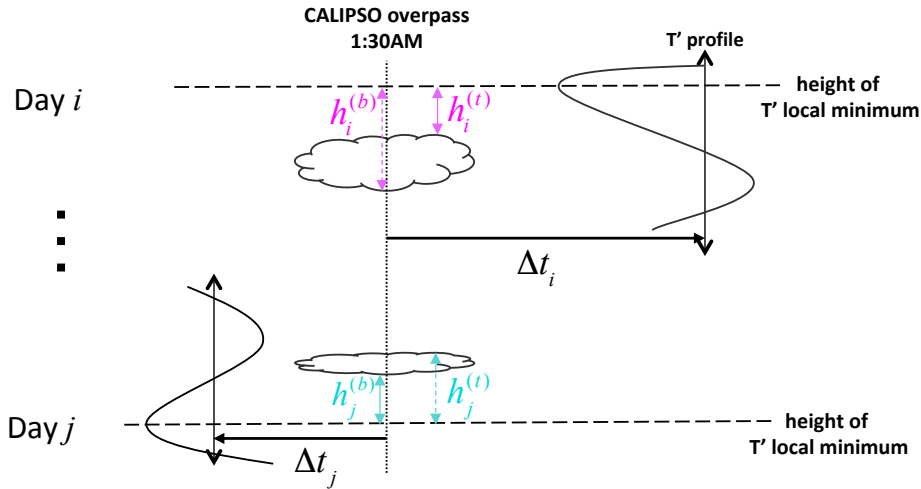
One difference between $\min(T')$ and $\max(T')$ is that the positive anomalies in $\min(T')$ occur below the altitude of
 $\min(T')$ while the negative anomalies in $\max(T')$ are centered on it. Most of the enhanced cloud occurrence occurs inside
300 Phase 1, and Phase 2 actually tends to have a negative cloud occurrence anomaly. Although the predictions of P18 suggests
that it may be more likely to find clouds in Phase 2 under low background RH_i , this global analysis suggests that on average
the role of Phase 1 in facilitating TTL clouds is dominant.

4.3 Comparison to P18

P18 suggests that (1) ice crystals within a confined range of r_e are suspended ~~approximately~~ in Phase 1 ~~and 2~~, and (2) for
305 low background relative humidity with respect to ice (RH_{ib}) ~~influences the phase at which these crystals are suspended.~~ the
confinement in Phase 1 may be positioned closer to Phase 2. These two features are depicted in their Figure 2. To evaluate
whether these predictions are consistent with satellite observations, we examine r_e and RH_{ib} in observations to see whether
these quantities exhibit any correlations to gravity waves clouds in each gravity wave phase. Although here we present analysis
motivated by P18, we note that their study assumes no background wind ~~nor~~ shear in their derivations and simulations.

310 Figure ??-10 shows normalized distributions of r_e in the four wave phases as well as their mean and standard deviation. These
distributions only contain nighttime 2C-ICE data, since the information toward thin cirrus are mostly from lidar backscatter.
Clouds above 17.5 km were omitted in this plot due to the low samples ($\sim 0.6\%$ of all TTL clouds). The distributions for
all phases are very similar regardless of height. In 14.5–15.5 and 15.5–16.5 km, the r_e distribution of Phase 1 has a peak
near 16 μm . Above 16.5 km this peak is not evident, but the Phase 1 distribution has higher values around 15 μm and lower
315 values between 20 to 25 μm , slightly differentiating Phase 1 from the other phases. The mean r_e of Phase 1 is lower than all
other three phases at all vertical layers, but the differences are small. Also, Phase 4 consistently has the largest r_e . In summary,
characteristics of r_e found here are qualitatively consistent with P18's findings, as Phase 1 tends to have a relative larger number

a) Instantaneous observations



b) Composite time

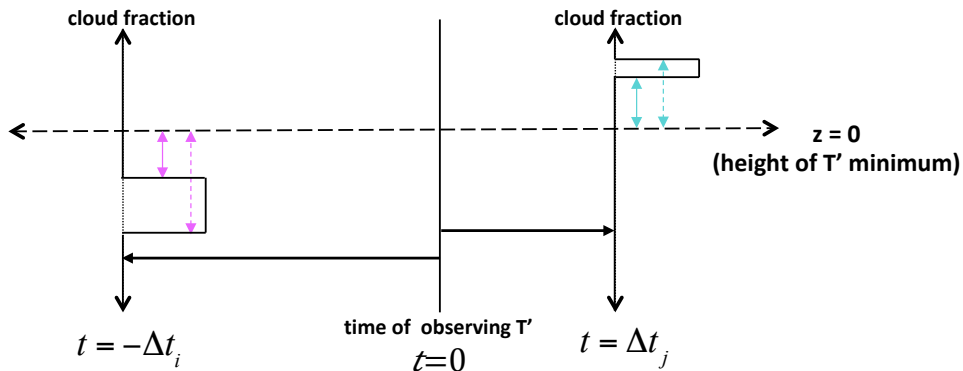


Figure 8. Schematic for creating the composite temporal evolution of cloud fraction with respect to T' minima. In this example, as shown in (a), during day i there is a collocated pair of CALIPSO and RO observations. The RO observation occurs Δt_i hours after that of CALIPSO, and the vertical distance between the height of local T' minimum and the cloud top and base is depicted by the dashed and solid magenta lines, respectively, with lengths $h_i^{(t)}$ and $h_i^{(b)}$. In the temporal compositing (b), in the time bin corresponding to Δt_i hours before observing T' , the cloud fraction is binned according to how much each vertical bin overlaps with the interval $[h_i^{(b)}, h_i^{(t)}]$. The same procedure is carried out for the collocated pair at day j . Also see text for explanation.

[slightly larger numbers](#) of ice particles localized around a certain r_e value. However we note that retrieving cloud properties of thin cirrus has large uncertainties and more research is needed to explore the r_e distribution in gravity waves phases using a variety of observations and models.

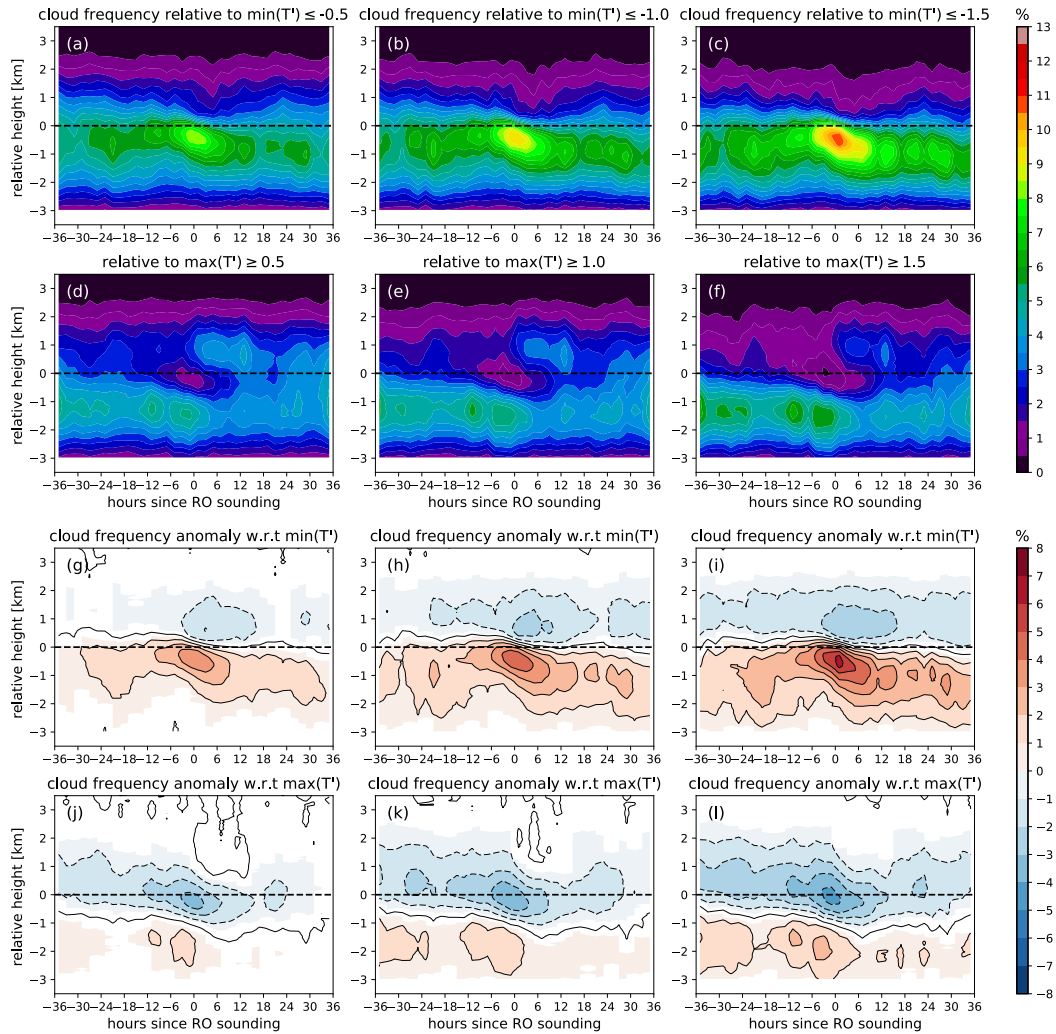


Figure 9. Composite of cloud frequency with respect to local minima (first row; [panels \(a\)-\(c\)](#)) or maxima (second row; [panels \(d\)-\(f\)](#)) of T' . The columns correspond to composites made from subsets of T' extrema with magnitudes greater or equal to 0.5 K (left column), 1.0 K (middle), and 1.5 K (right). Dashed horizontal [indicates lines indicate](#) the position of the local T' extrema. The third row [shows the background frequency \(see text for explanation\)](#). The fourth row [\(j\)-\(l\)](#) and fifth [fourth](#) rows [\(m\)-\(o\)](#) are the cloud frequencies anomalies associated with cold or warm anomalies, [calculated as the difference between the cloud frequency composites and the background cloud frequency respectively](#). Contours in the bottom two rows are at intervals of 1% (dashed negative), matching the filled color contours which show values at or above the 95% significance level.

As discussed in Section 4.1, K16 found that in the 2011 and 2013 flight legs over the Eastern Pacific there were slightly more clouds in Phase 2 than Phase 1, whereas in the 2014 flights over the Western Pacific a majority of clouds were in Phase 1. P18 argues that this may be due to the relatively low RH_{ib} characteristic of the TTL over the Eastern Pacific. P18 solved a simplified

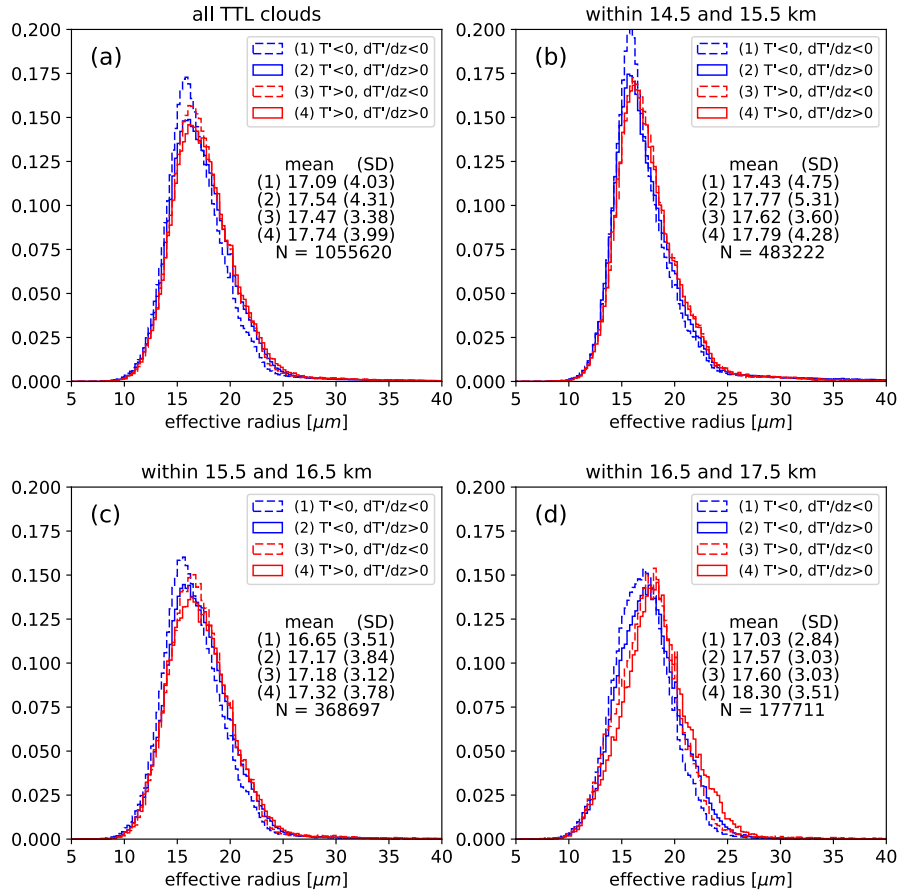


Figure 10. Normalized density function of r_e in each gravity wave phase for (a) all of TTL and (b)-(d) 1-km vertical layers. The mean and standard deviation (SD) of r_e in each phase and the total number of r_e samples (N) are given denoted in the legend.

set of equations describing the interaction of between gravity wave perturbations and ice particle growth/sedimentation. Comparison of the their solution using values of $RH_{ib} = 0.85$ or ~~0.64~~ 0.63 (to represent Western and Eastern Pacific, respectively) showed that the former results in the ice crystals being suspended in Phase 1 where in the latter ice particles were situated closer to the T' minimum which may result in more ice inside Phase 2. Motivated by these results we collocate the MLS water vapor retrieval to CALIPSO and RO data to evaluate whether observations suggest a similar dependence on RH_{ib} .

For each CALIPSO Cloud Profile bin identified as cloud, the collocated water vapor mixing ratio from the Aura MLS product is log-interpolated (as suggested by the product documentation) to the height of the cloud bin. To evaluate the saturation mixing ratio, we interpolate the 7-day mean temperature to the cloud height since we are interested in the RH_{ib} instead of the actual RH_i (which would include wave influence). The Goff-Gratch equation (Goff and Gratch, 1946) is used to get the saturation vapor pressure, and subsequently the saturation mixing ratio and RH_{ib} . ~~Figure ?? shows the cloud population in each phase partitioned by~~ Then the cloud bin is binned according to RH_{ib} values. ~~The subsets with RH_{ib} below 60%, between 60% to~~

335 ~~80%, and above~~ into bins of 0%, 50%, and then every 10% up to 180% ~~tend to have less clouds in Phase 1 compared to the other~~
~~. The first bin is wider due to the small amount of samples with very low RH_{ib} categories. The intermediate values, Figure~~
~~11 shows the cloud population in each phase as a function of RH_{ib} (between 80% to 120%) yielded the highest fractions in~~
~~Phase 1. Qualitatively, this show some consistency as well as the number of cloud bins in each RH_{ib} category. Compared to~~
340 ~~the relative humidity observed during the ATTREX campaign (Jensen et al., 2017), the values in our Figure 11 tends to be~~
~~high-biased. A possible cause of this is that we are estimating the relative humidity as coarse-resolution MLS mixing ratio~~
~~estimates divided by the saturation mixing ratio of the mean temperature. Due to the non-linearity of the Goff-Gratch equation,~~
~~the relative humidity evaluated this way will be larger than the actual average relative humidity.~~

~~Qualitatively, Figure 11 is consistent with P18 since there are more the Phase 2 percentage is higher when RH_{ib} is below~~
~~100%. The percentage of clouds in Phase 2 for the lowest two 1 also tends to increase with RH_{ib} categories, but we find only~~
345 ~~a slight dependence on up until RH_{ib} with no clear trend. We conclude that our analyses on r_e and $=100%$, above which there~~
~~is no appreciable trend between RH_{ib} does not prove or disprove to any of the phases. To summarize, our analysis of RH_{ib}~~
~~is consistent with P18's assertions but there is some qualitative consistency between P18 and our results findings, while the~~
~~results pertaining to r_e remain ambiguous.~~

5 Conclusions

350 This study uses multiple satellite datasets to evaluate the influence of gravity wave perturbations on TTL cirrus clouds. With
a focus on understanding the role of dT'/dz , the vertical gradient of the gravity wave temperature perturbation T' , we extract
 T' and dT'/dz from RO observations and collocate them to clouds observed by CALIPSO and 2C-ICE to understand cloud
occurrence and characteristics ~~relative to wave anomalies in distinct wave phases~~. Similar to the results of K16, we find that the
phase where T' and dT'/dz are both negative (Phase 1) is most frequently occupied by TTL clouds. The second most populous
355 phase is where $T' < 0$ and $dT'/dz > 0$ (Phase 2), followed by where $T' > 0$ and $dT'/dz < 0$ (Phase 3) and then $T' > 0$ and
 $dT'/dz > 0$ (Phase 4). We show that this relation among the four phases is more or less invariant with height or longitude.

A mean view of the temporal evolution of wave anomalies with respect to clouds is constructed by taking advantage of
RO's pseudo-random distribution in time and space. We collocate CALIPSO cloud observations to RO soundings that occur
before and after the CALIPSO observation, and by averaging a large number of observations with different time separations,
360 a composite time series of wave anomalies is presented. These composites show that, on average, the strongest cold anomaly
due to gravity waves tends to be centered on the height of cloud top, and this cold anomaly descends with time consistent with
the downward phase propagation of gravity and Kelvin waves ~~having with~~ upward group velocity.

In the cloud frequency composites made with respect to local T' minima or maxima, we find that the decrease of cloud
probability in the warm phase does not show clear dependence on the sign of dT'/dz . This is distinct from the cold phase,
365 where cloud probability is increased mainly below $\min(T')$ where dT'/dz is negative. Together with existing studies, this
result adds support to the idea that Phase 1 facilitates cloud formation and/or maintenance. Although the downward migration
of the increased cloud frequency may be due to ice sedimentation, this is unlikely to be the case for the decreased cloud

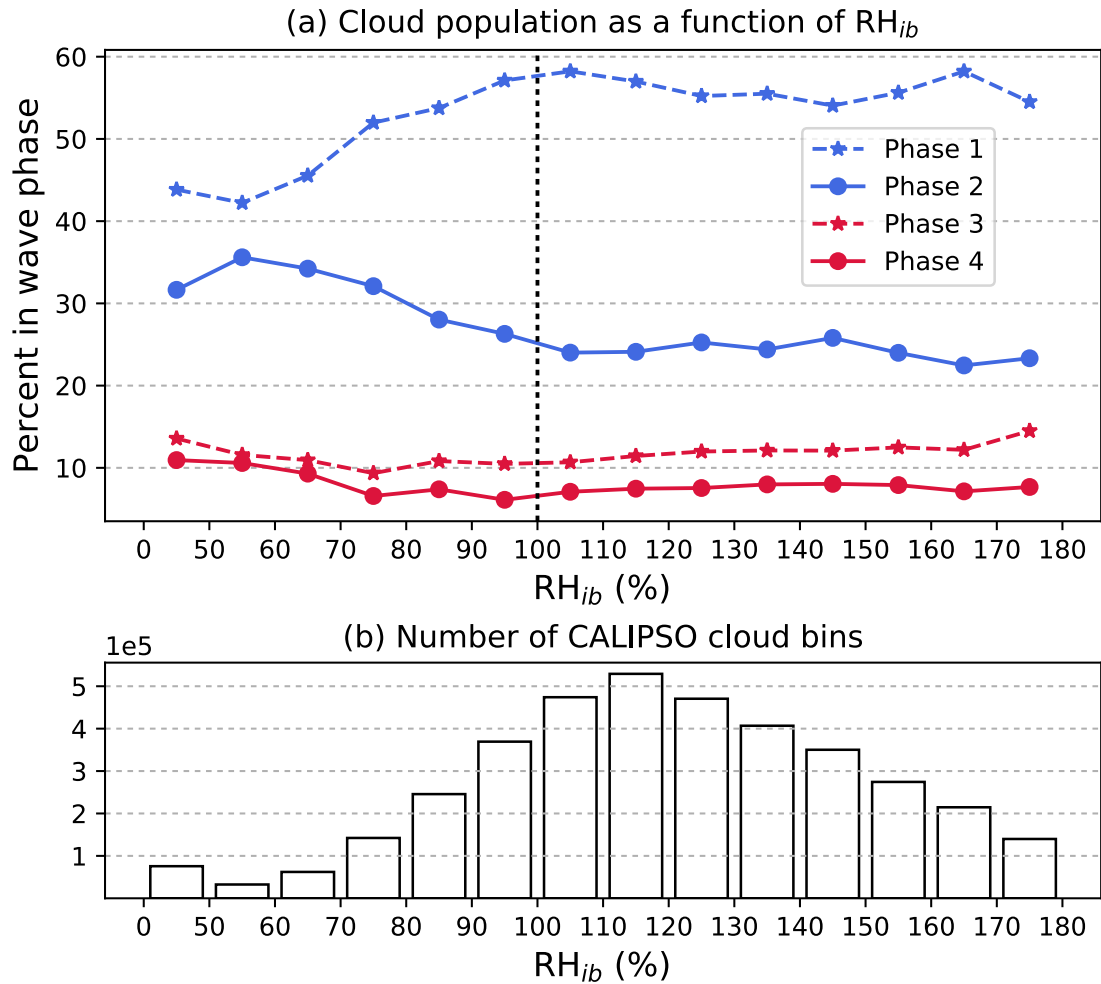


Figure 11. (a) Percentage of TTL clouds inside each wave phase categorized by as a function of background relative humidity with respect to ice (RH_{ib}). (b) Number of CALIPSO Cloud Profile bins in each RH_{ib} category.

frequency associated with the warm phase. Hence the downward migration of increased/decreased cloud frequency in the temporal composites is most likely due to waves with downward phase propagation. We also show that the positive or negative cloud frequency anomalies strengthen with increasing magnitude of T' minima or maxima, giving evidence on a global scale that the wave amplitude is connected to the probability of cloud occurrence.

Finally, using satellite estimates of r_e from 2C-ICE we assess the predictions of P18 which implies that one may observe a narrower distribution ice crystal effective radius inside Phase 1. Their conclusion that the background relative humidity with respect to ice affects the vertical position of clouds is also evaluated here by using RH_{ib} based on the Aura MLS H_2O product. Among all phases, r_e are distributed similarly but the distribution of Phase 1 had a notably sharper peak and than the other three

phases and also a slightly smaller mean r_e . The partitioning of cloud population among the four phases showed ~~some variation with different values of clear dependence on RH_{ib} , with Phase 1 having less clouds at very low or very high's cloud population increasing with RH_{ib} , but no clear trend is identified. Thus, while up until $RH_{ib}=100\%$. Overall,~~ our satellite-based analysis ~~has some show~~ qualitative consistency with the results of P18, ~~it is insufficient for verifying their assertions.~~

380 This study adds to the ~~exist findings literature~~ showing that Phase 1 has a distinct connection to TTL clouds. The findings of K16, based on aircraft data limited to specific regions and time span, have been extended by our study which shows that the large amount of clouds in Phase 1 is a general characteristic of the TTL. Based on our composite analysis using satellite data spanning ~~eight years (2007–2014)~~ seven years (2007–2013), the connection between wave anomalies and cloud occurrence is evident: cold anomalies are associated with the position of cloud top, and T' amplitudes influence the increase or decrease
385 in cloud frequency. The purpose of constructing composite temporal evolution by piecing together collocated temperature and cloud observations is an attempt to study processes occurring on a timescale typically unobserved by satellites. Although the resulting composites are not true time series, the ~~anomalies patterns depict signatures~~ anomaly patterns are consistent with wave propagation and enhances our understanding of how waves are connected to TTL clouds. It should be noted that although the composite technique shows a clear connection between wave anomalies and clouds, the technique is stationary in space; it
390 does not follow the position of clouds (moved by the background flow) nor the wave phase (moved as it propagates).

Due to the spatial and vertical resolution of the RO technique, the waves analyzed here have relatively large vertical wavelengths and low frequencies. ~~Despite this, the findings here should be important for TTL processes as Dzambo et al. (2019) shows~~ The vertical wavelength inferred from the anomalies in our composites is about 3 km. Dzambo et al. (2019) showed that the power spectrum of TTL gravity waves tend to peak at wavelengths of around 4–5 km, which is though at 3 km there is still
395 considerable power (their Figure 1). These wavelengths are all resolvable by RO soundings, so it can be assumed that this analysis has included a large part of the TTL gravity wave spectrum. Nevertheless, it remains to be explored whether the Phase 1 of high-frequency waves are also distinct from other phases. Also, possible explanations for Phase 1 favoring clouds remain an open question. Since negative dT'/dz corresponds to a ~~positive cooling rate (due to downward phase propagation as explained by K16),~~ upward wind anomaly as well as weakened stability, ~~as well as upward vertical motion wave anomalies~~
400 ~~(according to the gravity wave polarization relationships), it remains to be determined~~ whether one has a stronger role in ~~favoring clouds needs to be better understood~~ promoting cloud formation.

Data availability. The atmPrf radio occultation dataset can be obtained from the COSMIC Data Analysis and Archive Center (<https://cdaac-www.cosmic.ucar.edu/>). The Aura MLS Level 2 H₂O product is available from the Goddard Earth Sciences Data and Information Services Center (<https://disc.gsfc.nasa.gov>), and the 2C-ICE CloudSat/CALIPSO product is available on the CloudSat Data Processing Center
405 (www.cloudsat.cira.colostate.edu). The CALIPSO Level 2 Cloud Profile and Cloud Layer products are hosted on the NASA Atmospheric Science Data Center (<https://eosweb.larc.nasa.gov>).

Appendix A: Calculation of background cloud frequency for Figure 9

A1

410 The cloud frequency composites in the top two rows of Figure 9 are made using the altitude of the T' extrema as the zero height. To generate a composite where the vertical position of T' extrema has no relationship with cloud top/base height, for each T' extremum we generate a random altitude using uniform distribution $unif(14.5, 18.5)$ and make a separate cloud frequency time-height composite with the random altitude as zero height. The resulting cloud frequency height-time distribution is regarded as the 'background' distribution. The difference between this background and the cloud frequency composites in Figure 9 (a)-(f) are then the anomalies associated with local T' minimum or maximum. The anomalies derived in this way are
415 shown in Figure 9 (g)-(l).

The distribution of cloud fraction in each time-height bin is similar to those shown in Figure 5 and therefore is not normal, so the Student's t-test cannot be used for statistical testing. We use the two-sided two-sample Kolmogorov-Smirnov test which does not make any assumptions about the data distributions. This test can be used to evaluate whether two discrete probability distributions differ from each other. The null hypothesis is that the cloud frequency pattern composited on T' minima/maxima
420 (first/second row of Figure 9) is not different than the randomly generated 'background' cloud frequency pattern.

Author contributions. KC designed and performed the study with suggestions from TL. Both authors contributed to the writing of this article.

Competing interests. The authors declare no conflicts of interest.

Acknowledgements. This study was supported by the NASA Earth and Space Sciences Fellowship 80NSSC17K0384. We thank Sergey Sokolovskiy and Zhen Zeng for comments regarding the usage of radio occultation data and William Read regarding the Aura MLS H₂O
425 product.

References

- Alexander, S. P., Tsuda, T., Kawatani, Y., and Takahashi, M.: Global distribution of atmospheric waves in the equatorial upper troposphere and lower stratosphere: COSMIC observations of wave mean flow interactions, *Journal of Geophysical Research Atmospheres*, 113, 1–18, <https://doi.org/10.1029/2008JD010039>, 2008.
- 430 Anthes, R. A., Bernhardt, P. A., Chen, Y., Cucurull, L., Dymond, K. F., Ector, D., Healy, S. B., Ho, S.-P., Hunt, D. C., Kuo, Y.-H., Liu, H., Manning, K., McCormick, C., Meehan, T. K., Randel, W. J., Rocken, C., Schreiner, W. S., Sokolovskiy, S. V., Syndergaard, S., Thompson, D. C., Trenberth, K. E., Wee, T.-K., Yen, N. L., and Zeng, Z.: The COSMIC/FORMOSAT-3 Mission: Early Results, *Bulletin of the American Meteorological Society*, 89, 313–334, <https://doi.org/10.1175/BAMS-89-3-313>, <http://journals.ametsoc.org/doi/10.1175/BAMS-89-3-313>, 2008.
- 435 Banerjee, A., Chiodo, G., Previdi, M., Ponater, M., Conley, A. J., and Polvani, L. M.: Stratospheric water vapor: an important climate feedback, *Climate Dynamics*, 0, 1–14, <https://doi.org/10.1007/s00382-019-04721-4>, <https://link.springer.com/article/10.1007/s00382-019-04721-4>, 2019.
- Deng, M., Mace, G. G., Wang, Z., and Paul Lawson, R.: Evaluation of several A-Train ice cloud retrieval products with in situ measurements collected during the SPARTICUS campaign, *Journal of Applied Meteorology and Climatology*, 52, 1014–1030, <https://doi.org/10.1175/JAMC-D-12-054.1>, 2013.
- 440 Deng, M., Mace, G. G., Wang, Z., and Berry, E.: Cloudsat 2C-ICE product update with a new Ze parameterization in lidar-only region, *Journal of Geophysical Research*, 120, 12,198–12,208, <https://doi.org/10.1002/2015JD023600>, 2015.
- Dzambo, A. M., Hitchman, M. H., and Chang, K. W.: The influence of gravity waves on ice saturation in the tropical tropopause layer over darwin, Australia, *Atmosphere*, 10, <https://doi.org/10.3390/ATMOS10120778>, 2019.
- 445 Foelsche, U., Scherllin-Pirscher, B., Ladstädter, F., Steiner, A. K., and Kirchengast, G.: Refractivity and temperature climate records from multiple radio occultation satellites consistent within 0.05%, *Atmospheric Measurement Techniques*, 4, 2007–2018, <https://doi.org/10.5194/amt-4-2007-2011>, 2011.
- Fujiwara, M., Iwasaki, S., Shimizu, A., Inai, Y., Shiotani, M., Hasebe, F., Matsui, I., Sugimoto, N., Okamoto, H., Nishi, N., Hamada, A., Sakazaki, T., and Yoneyama, K.: Cirrus observations in the tropical tropopause layer over the western Pacific, *Journal of Geophysical Research Atmospheres*, 114, 1–23, <https://doi.org/10.1029/2008JD011040>, 2009.
- 450 Goff, J. A. and Gratch, S.: Low-pressure properties of water from -160 to 212 °F, in: *Transactions of the American Society of Heating and Ventilating Engineers*, New York, pp. 95–122, 1946.
- Highwood, E. J. and Hoskins, B. J.: The tropical tropopause, *Quarterly Journal of the Royal Meteorological Society*, 124, 1579–1604, <https://doi.org/10.1002/qj.49712454911>, <http://doi.wiley.com/10.1002/qj.49712454911>, 1998.
- 455 Hollander, M., A. Wolfe, D., and Chicken, E.: *Nonparametric Statistical Methods*, Wiley Series in Probability and Statistics, Wiley, third edit edn., <https://doi.org/10.1002/9781119196037>, <https://onlinelibrary.wiley.com/doi/book/10.1002/9781119196037>, 2015.
- Holton, J. R., Haynes, P. H., McIntyre, M. E., Douglass, A. R., Rood, R. B., and Pfister, L.: Stratosphere-troposphere exchange, *Reviews of Geophysics*, 33, 403, <https://doi.org/10.1029/95RG02097>, <http://doi.wiley.com/10.1029/95RG02097>, 1995.
- 460 Immler, F., Krüger, K., Tegtmeier, S., Fujiwara, M., Fortuin, P., Verver, G., and Schrems, O.: Cirrus clouds, humidity, and dehydration in the tropical tropopause layer observed at Paramaribo, Suriname (5.8°N, 55.2°W), *Journal of Geophysical Research Atmospheres*, 112, 1–14, <https://doi.org/10.1029/2006JD007440>, 2007.

- Jensen, E. J., Diskin, G., Lawson, R. P., Lance, S., Bui, T. P., Hlavka, D., McGill, M., Pfister, L., Toon, O. B., and Gao, R.: Ice nucleation and dehydration in the Tropical Tropopause Layer, *Proceedings of the National Academy of Sciences*, 110, 2041–2046, <https://doi.org/10.1073/pnas.1217104110>, <http://www.pnas.org/content/110/6/2041><http://www.pnas.org/cgi/doi/10.1073/pnas.1217104110>, 2013.
- 465
- Jensen, E. J., Thornberry, T. D., Rollins, A. W., Ueyama, R., Pfister, L., Bui, T., Diskin, G. S., Digangi, J. P., Hints, E., Gao, R. S., Woods, S., Lawson, R. P., and Pittman, J.: Physical processes controlling the spatial distributions of relative humidity in the tropical tropopause layer over the Pacific, *Journal of Geophysical Research*, 122, 6094–6107, <https://doi.org/10.1002/2017JD026632>, 2017.
- Kim, J.-E., Alexander, M. J., Bui, T. P., Dean-Day, J. M., Lawson, R. P., Woods, S., Hlavka, D., Pfister, L., and Jensen, E. J.: Ubiquitous influence of waves on tropical high cirrus clouds, *Geophysical Research Letters*, 43, 5895–5901, <https://doi.org/10.1002/2016GL069293>, <http://doi.wiley.com/10.1002/2016GL069293>, 2016.
- 470
- Kursinski, E. R., Hajj, G. A., Schofield, J. T., Linfield, R. P., and Hardy, K. R.: Observing Earth’s atmosphere with radio occultation measurements using the Global Positioning System, *Journal of Geophysical Research: Atmospheres*, 102, 23 429–23 465, <https://doi.org/10.1029/97JD01569>, <http://doi.wiley.com/10.1029/97JD01569>, 1997.
- 475
- Lambert, A., Read, W. G., Livesey, N. J., Santee, M. L., Manney, G. L., Froidevaux, L., Wu, D. L., Schwartz, M. J., Pumphrey, H. C., Jimenez, C., Nedoluha, G. E., Cofield, R. E., Cuddy, D. T., Daffer, W. H., Drouin, B. J., Fuller, R. A., Jarnot, R. F., Knosp, B. W., Pickett, H. M., Perun, V. S., Snyder, W. V., Stek, P. C., Thurstans, R. P., Wagner, P. A., Waters, J. W., Jucks, K. W., Toon, G. C., Stachnik, R. A., Bernath, P. F., Boone, C. D., Walker, K. A., Urban, J., Murtagh, D., Elkins, J. W., and Atlas, E.: Validation of the Aura Microwave Limb Sounder middle atmosphere water vapor and nitrous oxide measurements, *Journal of Geophysical Research*, 112, D24S36, <https://doi.org/10.1029/2007JD008724>, <http://doi.wiley.com/10.1029/2007JD008724>, 2007.
- 480
- Livesey, N. J., Read, W. G., Wagner, P. A., Froidevaux, L., Lambert, A., Manney, G. L., Valle, L. F. M., Pumphrey, H. C., Santee, M. L., Schwartz, M. J., Wang, S., Fuller, R. A., Jarnot, R. F., Knosp, B. W., Martinez, E., and Lay, R. R.: Version 4.2 x Level 2 data quality and description document, JPL D-33509 Rev. C, Jet Propulsion Laboratory, [https://mls.jpl.nasa.gov/data/v4-2/{_}data{_\]quality{_\]document.pdf](https://mls.jpl.nasa.gov/data/v4-2/{_}data{_]quality{_]document.pdf), 2017.
- 485
- Masunaga, H.: A Satellite Study of the Atmospheric Forcing and Response to Moist Convection over Tropical and Subtropical Oceans, *Journal of the Atmospheric Sciences*, 69, 150–167, <https://doi.org/10.1175/JAS-D-11-016.1>, <http://journals.ametsoc.org/doi/abs/10.1175/JAS-D-11-016.1>, 2012.
- Masunaga, H. and L’Ecuyer, T. S.: A Mechanism of Tropical Convection Inferred from Observed Variability in the Moist Static Energy Budget, *Journal of the Atmospheric Sciences*, 71, 3747–3766, <https://doi.org/10.1175/JAS-D-14-0015.1>, <http://journals.ametsoc.org/doi/abs/10.1175/JAS-D-14-0015.1>, 2014.
- 490
- Paulik, L. C. and Birner, T.: Quantifying the deep convective temperature signal within the tropical tropopause layer (TTL), *Atmospheric Chemistry and Physics*, 12, 12 183–12 195, <https://doi.org/10.5194/acp-12-12183-2012>, <http://www.atmos-chem-phys.net/12/12183/2012/>, 2012.
- Pirscher, B., Foelsche, U., Borsche, M., Kirchengast, G., and Kuo, Y.-H.: Analysis of migrating diurnal tides detected in FORMOSAT-3/COSMIC temperature data, *Journal of Geophysical Research*, 115, D14 108, <https://doi.org/10.1029/2009JD013008>, <http://doi.wiley.com/10.1029/2009JD013008>, 2010.
- 495
- Ploeger, F., Gottschling, C., Griessbach, S., Groß, J. U., Guenther, G., Konopka, P., Müller, R., Riese, M., Stroh, F., Tao, M., Ungermann, J., Vogel, B., and Von Hobe, M.: A potential vorticity-based determination of the transport barrier in the Asian summer monsoon anticyclone, *Atmospheric Chemistry and Physics*, 15, 13 145–13 159, <https://doi.org/10.5194/acp-15-13145-2015>, 2015.

- 500 Podglajen, A., Plougonven, R., Hertzog, A., and Jensen, E.: Impact of gravity waves on the motion and distribution of atmospheric ice particles, *Atmospheric Chemistry and Physics*, 18, 10799–10823, <https://doi.org/10.5194/acp-18-10799-2018>, 2018.
- Ramage, C. S.: Role of a tropical “Maritime Continent” in the atmospheric circulation, *Monthly Weather Review*, 96, 365–370, [https://doi.org/10.1175/1520-0493\(1968\)096<0365:ROATMC>2.0.CO;2](https://doi.org/10.1175/1520-0493(1968)096<0365:ROATMC>2.0.CO;2), <http://journals.ametsoc.org/doi/abs/10.1175/1520-0493%281968%29096%3C0365%3AROATMC%3E2.0.CO%3B2>, 1968.
- 505 Randel, W. J. and Wu, F.: Kelvin wave variability near the equatorial tropopause observed in GPS radio occultation measurements, *Journal of Geophysical Research D: Atmospheres*, 110, 1–13, <https://doi.org/10.1029/2004JD005006>, 2005.
- Read, W. G., Lambert, A., Bacmeister, J., Cofield, R. E., Christensen, L. E., Cuddy, D. T., Daffer, W. H., Drouin, B. J., Fetzer, E., Froidevaux, L., Fuller, R., Herman, R., Jarnot, R. F., Jiang, J. H., Jiang, Y. B., Kelly, K., Knosp, B. W., Kovalenko, L. J., Livesey, N. J., Liu, H.-C., Manney, G. L., Pickett, H. M., Pumphrey, H. C., Rosenlof, K. H., Sabouchi, X., Santee, M. L., Schwartz, M. J., Snyder, W. V., Stek, P. C.,
- 510 Su, H., Takacs, L. L., Thurstans, R. P., Vömel, H., Wagner, P. A., Waters, J. W., Webster, C. R., Weinstock, E. M., and Wu, D. L.: Aura Microwave Limb Sounder upper tropospheric and lower stratospheric H₂O and relative humidity with respect to ice validation, *Journal of Geophysical Research*, 112, D24S35, <https://doi.org/10.1029/2007JD008752>, <http://doi.wiley.com/10.1029/2007JD008752>, 2007.
- Sassen, K., Wang, Z., and Liu, D.: Cirrus clouds and deep convection in the tropics: Insights from CALIPSO and CloudSat, *Journal of Geophysical Research Atmospheres*, 114, 1–11, <https://doi.org/10.1029/2009JD011916>, 2009.
- 515 Sauter, K., L’Ecuyer, T. S., den Heever, S. C., Twohy, C., Heidinger, A., Wanzong, S., and Wood, N.: The Observed Influence of Tropical Convection on the Saharan Dust Layer, *Journal of Geophysical Research: Atmospheres*, p. 2019JD031365, <https://doi.org/10.1029/2019JD031365>, <https://onlinelibrary.wiley.com/doi/abs/10.1029/2019JD031365>, 2019.
- Scherllin-Pirscher, B., Randel, W. J., and Kim, J.: Tropical temperature variability and Kelvin-wave activity in the UTLS from GPS RO measurements, *Atmospheric Chemistry and Physics*, 17, 793–806, <https://doi.org/10.5194/acp-17-793-2017>, 2017.
- 520 Schoeberl, M. R., Jensen, E. J., and Woods, S.: Gravity waves amplify upper tropospheric dehydration by clouds, *Earth and Space Science*, 2, 485–500, <https://doi.org/10.1002/2015EA000127>, <http://doi.wiley.com/10.1002/2015EA000127>, 2015.
- Solomon, S., Rosenlof, K. H., Portmann, R. W., Daniel, J. S., Davis, S. M., Sanford, T. J., and Plattner, G.-K.: Contributions of Stratospheric Water Vapor to Decadal Changes in the Rate of Global Warming, *Science*, 327, 1219–1223, <https://doi.org/10.1126/science.1182488>, <http://www.sciencemag.org/cgi/doi/10.1126/science.1182488>, 2010.
- 525 Suzuki, J., Fujiwara, M., Nishizawa, T., Shirooka, R., Yoneyama, K., Katsumata, M., Matsui, I., and Sugimoto, N.: The occurrence of cirrus clouds associated with eastward propagating equatorial $n = 0$ inertio-gravity and Kelvin waves in November 2011 during the CINDY2011/DYNAMO campaign, *Journal of Geophysical Research Atmospheres*, 118, 12941–12947, <https://doi.org/10.1002/2013JD019960>, 2013.
- Von Engel, A., Healy, S., Marquardt, C., Andres, Y., and Sancho, F.: Validation of operational GRAS radio occultation data, *Geophysical Research Letters*, 36, 5–8, <https://doi.org/10.1029/2009GL039968>, 2009.
- 530 Wickert, J., Reigber, C., Beyerle, G., König, R., Marquardt, C., Schmidt, T., Grunwaldt, L., Galas, R., Meehan, T. K., Melbourne, W. G., and Hocke, K.: Atmosphere sounding by GPS radio occultation: First results from CHAMP, *Geophysical Research Letters*, 28, 3263–3266, <https://doi.org/10.1029/2001GL013117>, <http://doi.wiley.com/10.1029/2001GL013117>, 2001.
- Winker, D. M., Pelon, J., Coakley, J. A., Ackerman, S. A., Charlson, R. J., Colarco, P. R., Flamant, P., Fu, Q., Hoff, R. M., Kittaka, C.,
- 535 Kubar, T. L., Le Treut, H., McCormick, M. P., Mégie, G., Poole, L., Powell, K., Trepte, C., Vaughan, M. A., and Wielicki, B. A.: The CALIPSO Mission, *Bulletin of the American Meteorological Society*, 91, 1211–1230, <https://doi.org/10.1175/2010BAMS3009.1>, <http://journals.ametsoc.org/doi/10.1175/2010BAMS3009.1>, 2010.

- 540 Zeng, Z., Randel, W., Sokolovskiy, S., Deser, C., Kuo, Y.-H., Hagan, M., Du, J., and Ward, W.: Detection of migrating diurnal tide in the tropical upper troposphere and lower stratosphere using the Challenging Minisatellite Payload radio occultation data, *Journal of Geophysical Research*, 113, D03 102, <https://doi.org/10.1029/2007JD008725>, <http://doi.wiley.com/10.1029/2007JD008725>, 2008.
- Zeng, Z., Sokolovskiy, S., Schreiner, W. S., and Hunt, D.: Representation of vertical atmospheric structures by radio occultation observations in the upper troposphere and lower stratosphere: Comparison to high-resolution radiosonde profiles, *Journal of Atmospheric and Oceanic Technology*, 36, 655–670, <https://doi.org/10.1175/JTECH-D-18-0105.1>, 2019.